mGluR5 PAMs rescue cortical and behavioural defects in a mouse model of CDKL5 deficiency disorder.

Antonia Gurgone[1], Riccardo Pizzo[1], Alessandra Raspanti[1], Giuseppe Chiantia[1], Sunaina Devi[1], Noemi Morello[1], Federica Pilotto[1], Sara Gnavi[1], Leonardo Lupori[2], Raffaele Mazziotti[3], Giulia Sagona[3], Elena Putignano[4], Alessio Nocentini[5], Claudiu Supuran[5], Andrea Marcantoni[6], Tommaso Pizzorusso[2,4] and Maurizio Giustetto[1*]

[1]Rita Levi-Montalcini" Department of Neuroscience, University of Turin, Turin (Italy); [2]BIO@SNS lab, Scuola Normale Superiore, 56124 Pisa, Italy; [3]Department of Developmental Neuroscience, IRCCS Stella Maris Foundation, 56128 Pisa, Italy, [4]Institute of Neuroscience, CNR, 56124 Pisa, Italy; [5]NEUROFARBA Department, Section of Pharmaceutical and Nutraceutical Sciences, University of Florence, 50019 Sesto Fiorentino (Florence), Italy. [6]Department of Drug Science and "NIS" Inter-departmental Centre, University of Turin, Turin, Italy.

*Correspondence: maurizio.giustetto@unito.it

Università di Torino, Dipartimento di Neuroscienze "Rita Levi Montalcini"

Corso Raffaello 30; 10125 Torino - ITALY

Tel. +39-011-670-7725 (office); +39-011-670-7731 (lab)

Abstract

Cyclin-dependent kinase-like 5 (CDKL5) deficiency disorder (CDD) is a rare neurodevelopmental disease without a cure, caused by mutations in a serine/threonine kinase highly expressed in the forebrain. CDD is characterized by early-onset seizures, severe intellectual disabilities, autistic-like traits, sensorimotor and cortical visual impairments (CVI). The urgent need to find a therapy for the CCD induced our group to search novel druggable targets with relevant synaptic function and which modulation could restore most of the defects shown by CDD patients. Specifically, we focus on the metabotropic glutamate receptor 5 (mGluR5), a receptor whose activity is regulated by the interaction with Homer1bc, a scaffolding protein downregulated in CDKL5$^{-/y}$ mice. By performing *in-vivo* and *in-vitro* experiments we found that CDKL5 loss tampers with the interaction between the mGluR5 and Homer1bc leading to an aberrant expression and function of this receptor. These mGluR5 defects induced a defective modulation of NMDAR currents and an aberrant excitatory synaptic transmission. Our results also suggest that a positive modulation of the mGluR5, with specific allosteric modulators (PAMs) as CDPPB and RO6807794, could restore synaptic, functional and behavioural defects shown by CDD mouse model. Intriguingly, CDD post-mortem human brains share similar synaptic defects with Cdkl5-/y mice and a mGluR5 PAM ameliorates morphofunctional, behavioral and CVI impairments in mutant mice, a sign correlating with developmental delay in CDD patients. Our results unveil a promising druggable target that could be extensively explored to find a new therapeutic strategy for CDD patients.

Keywords: CDKL5 deficiency disorder; group I metabotropic glutamate receptors; positive allosteric modulators; NMDA-mediated current.

1. Introduction

CDKL5 is a serine/threonine kinase highly expressed especially in the forebrain during the peak of synaptogenesis (Rusconi et al., 2008). CDKL5 phosphorylates several substrates and is involved in a broad variety of cellular processes such as gene expression, neuronal migration, axon outgrowth, dendritic morphogenesis, synapses development and function (Baltussen et al., 2018; Muñoz et al., 2018; Nawaz et al., 2016; Trazzi et al., 2016). In the nucleous CDKL5 has been shown to interact with epigenetic factors, such as methyl-CpG-binding protein 2 (MeCP2) and DNA Methyltransferase 1 (DNMT1) (Kameshita et al., 2008; Mari et al., 2005), suggesting a still unclear role of CDKL5 in regulating gene activation. Recently, several cytoplasmic targets of CDKL5 phosphorylation, including MAP1S, EB2 and ARHGEF2, have been identified pointing to a major role of this kinase in the control of cytoskeletal function. Moreover, CDKL5 has been found to accumulate at synapses where it can interact with the palmitoylated form of postsynaptic density protein 95 (PSD-95) (Zhu et al., 2013). The interaction with PSD95 facilitates the phosphorylation of the adhesion molecule netrin-G1 ligand (NGL-1) (Ricciardi et al., 2012) a step that promotes the maturation of dendritic spines, i.e., the vast majority of glutamatergic postsynaptic sites in the forebrain, as well as the formation and function of excitatory connections. In addition, Barbiero et al. (2017) (Barbiero et al., 2017) showed that IQ motif containing GTPase activating protein 1 (IQGAP1) can interact with CDKL5 and thus mediate the formation of complexes with post-synaptic proteins such as PSD-95 or both AMPA- and NMDA-glutamatergic receptors. Interestingly, shRNA-mediated knockdown of CDKL5 can influence the synaptic expression of the GluA2 subunit (Tramarin et al., 2018) further highlighting that the involvement of CDKL5 in glutamatergic neurotransmission is yet to be unfolded.

To study the consequences of the lack of CDKL5 *in-vivo,* different CDKL5-KO mouse lines have been recently generated (Amendola et al., 2014; Okuda et al., 2017; Wang et al., 2012). They all display a broad spectrum of behavioural abnormalities, including hind-limb clasping, motor

hyperactivity, abnormal eye tracking, impaired learning and memory, and autistic-like phenotypes (Okuda et al., 2017), closely modelling human CDD (S. Demarest et al., 2019). Moreover, sensory defects such as tactile, visual and auditory impairments were recently revealed in CDD mouse models (Mazziotti et al., 2017; Pizzo et al., 2019; Wang et al., 2012). For example, cortical visual impairment (CVI), that is correlated with developmental delay in CDD patients (S. Demarest et al., 2019), is found in CDKL5 mutant mice starting from P27-P28 both in heterozygous and homozygous animals (Mazziotti et al., 2017; Wang et al., 2012).

Aberrant sensory processing in mice lacking CDKL5 is associated with severe abnormalities of the cerebral cortex, including altered dendritic arborization of pyramidal neurons, the downregulation of the postsynaptic scaffolding proteins PSD95 and Homer, and the disruption of AKT–mTOR signaling (Amendola et al., 2014; Della Sala et al., 2016; Pizzo et al., 2016; Wang et al., 2012). Moreover, we revealed that CDKL5 plays a key role in the dynamic of dendritic spines turn-over in the primary somatosensory (S1) cortex (Della Sala et al., 2016) by promoting their stabilization. In addition, S1 cortex of CDKL5$^{-/y}$ mice show impaired excitatory synaptic transmission and maintenance of long-term potentiation induced by theta-burst stimulation, emphasizing the role of CDKL5 in excitatory cortical connectivity (Della Sala et al., 2016; Pizzo et al., 2019).

Given all the above, we reasoned that by identifying druggable targets with relevant synaptic function is of pivotal importance to uncover novel therapeutic options for CDD. Here we report that both the expression and function of a member of group I metabotropic glutamate receptors, mGluR5, are abnormal in CDKL5$^{-/y}$ mice cerebral cortex and that the administration of selective mGluR5 positive allosteric modulators (PAMs) can rescue synaptic, cellular, and behavioural defects shown by mutant mice.

2. Results

2.1. Altered mGluR5/Homer1bc organization in the cerebral cortex of Cdkl5$^{-/y}$ mice.

We focused the analyses on mGluR5 guided by mounting evidence pointing at their role in critical mechanisms involved in CDD such as synaptogenesis, dendritic spines formation/maturation and synaptic plasticity (Ballester-Rosado et al., 2016; Chen et al., 2012; Edfawy et al., 2019; Piers et al., 2012). Because to exert its signaling functions within the PSD mGluR5 needs to interact with Homer1bc (Giuffrida et al., 2005; Ronesi et al., 2012; Scheefhals and MacGillavry, 2018; Tu et al., 1999) which is downregulated in the cortex of CDKL5$^{-/y}$ mice (Pizzo et al., 2019, 2016), we evaluated the strength of mGlur5-Homer1bc binding in mutant mice. Intriguingly, co-immunoprecipitation (co-IP) assays of cortical synaptosomal fraction (fig.1A) revealed that the amount of mGluR5 immunoprecipitated with Homer1bc is significantly reduced in Cdkl5$^{-/y}$ mice compared to Cdkl5$^{+/y}$ animals (O.D mGluR5/Homer1bc * $p < 0.05$; fig 1B). We next assessed mGluR5 expression in the neuropil by performing immunofluorescence experiments on S1 cortices from Cdkl5$^{-/y}$ and Cdkl5$^{+/y}$ mice (fig. 1C). By using a fixation/staining protocol improved for postsynaptic protein localization (Morello et al., 2018; Pizzo et al., 2016), mGluR5 immunofluorescence (fig. 1C) resulted in discrete puncta that were found closely localized, but only rarely overlapping, with PSD-95^{+} puncta in agreement with previously reported perisynaptic localization of mGluR5 (Lujan et al., 1996). Interestingly, the quantitative analysis (fig. 1D) revealed that mGluR5-puncta density is strongly reduced in layers II-III and V of somatosensory (S1) cortex in Cdkl5$^{-/y}$ mice compared to controls (layers II-III and layer V: Cdkl5$^{+/y}$ vs Cdkl5$^{-/y}$ $p < 0.05$; fig. 1C-D). These findings indicate that the presence of CDKL5 is required for both mGluR5-Homer1bc binding and the synaptic localization of mGluR5.

Fig.1

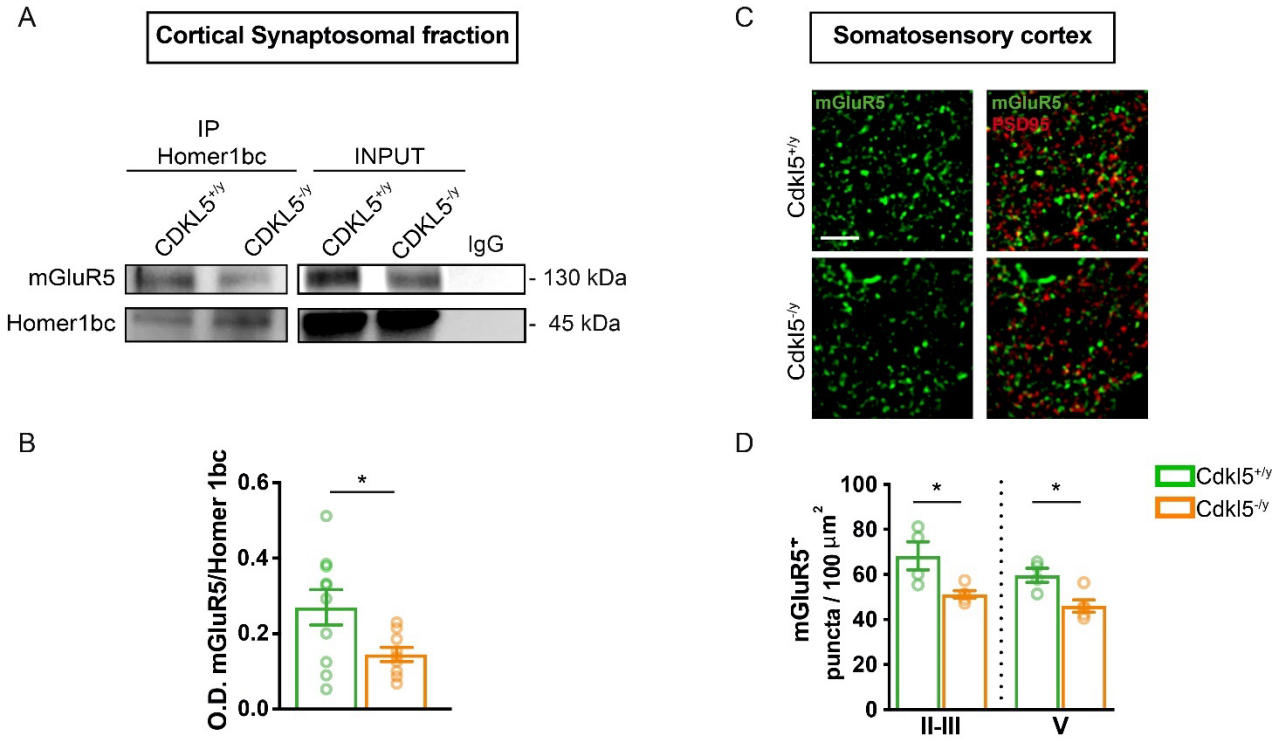

Figure 1. CDKL5 loss is responsible for both the disruption of mGluR5-Homer1bc interaction and the reduction of mGluR5 localization in the cortical neuropil. *(**A**) Co-IP of cortical synaptosomal fraction (P2) from P56 mice by using anti-Homer1bc. IgG: control lane in the absence of antibodies. Immunoprecipitates and inputs were analyzed by immunoblotting for mGluR5 and Homer1bc. (**B**) Histograms showing Co-IP quantitation expressed as optical density (O.D.). (**C**) Confocal microscopy images showing mGluR5^{+} (green) and PSD-95^{+} (red) immunopuncta in layers II/III of S1 cortex (scale bar: 5 µm). (**D**) Histograms displaying the density of mGluR5^{+} puncta. Student T test *p < 0.05 (Co-IP: n = 8 IFL: n = 4).*

2.2 mGluR5-mediated synaptic signaling is severely disrupted in Cdkl5$^{-/y}$ cortical neurons.

The reduced mGluR5-Homer1bc association that we found suggests that the receptor activity might be compromised (Aloisi et al., 2017; Kammermeier and Worley, 2007). To test this idea, we started by recording spontaneous miniature excitatory postsynaptic currents (mEPSCs) in neuronal cultures of the S1 cortex from both Cdkl5$^{+/y}$ and Cdkl5$^{-/y}$ mice (fig. 2A-D, upper part), before and after

mGluR5 activation. As we reported in a previous study (Della Sala et al., 2016), mEPSCs recorded from CDKL5 null neurons showed an increased inter-event interval (IEI) than WT neurons ($Cdkl5^{+/y}$ vs $Cdkl5^{-/y}$ $p < 0.05$; fig. 2D) while the peak mean amplitude was similar between genotypes ($Cdkl5^{+/y}$ vs $Cdkl5^{-/y}$ $p > 0.05$; fig. 2C). Intriguingly, we found that when cortical neurons were stimulated for two minutes with the selective mGluR5 agonist DHPG (100 μm), mEPSCs frequency was significantly increased in $Cdkl5^{+/y}$ cultures (fig. 2E, lower part; A) (Moult et al., 2006; Verpelli et al., 2011), but not in $Cdkl5^{-/y}$ neurons (fig. 2E) suggesting a negative impact of CDKL5 loss on mGluR5 signaling in excitatory synaptic transmission. Next, we performed whole-cell patch-clamp recordings in S1 cortex neuronal cultures and NMDA currents elicited by concurrent mGluR5 activation were recorded as in Reiner et al., 2018 (Reiner and Levitz, 2018). At first, we measured the average inward current activated by administration of NMDA (50 mM) (I_{NMDA}). Strikingly, $Cdkl5^{-/y}$ cultures showed a robust reduction of I_{NMDA} with respect to $Cdkl5^{+/y}$ neurons (fig. 2F, upper part) resulting in a statistically significant change ($Cdkl5^{+/y}$: 869.6 ± 85.4 pA, $Cdkl5^{-/y}$: 544.2 ± 113.2 pA; $p < 0.01$; fig. 2G). Next, we assessed I_{NMDA} after a 2 min application of DHPG (100 μm) before NMDA administration. As expected, we found that DHPG increased I_{NMDA} in $Cdkl5^{+/y}$ cells, (fig. 2F, lower part; see also Vicidomini et al., 2017)) while, interestingly, it produced no effect in $Cdkl5^{-/y}$ neurons (fig. 2F, lower part), as illustrated by the sharp difference in the percentage of I_{NMDA} change between genotypes ($Cdkl5^{+/y}$: 38.35%; $Cdkl5^{-/y}$: –14.47%, $p < 0.05$. Fig. 2H). Furthermore, while 73% of WT cortical neurons (11/15 cells) showed potentiated I_{NMDA} after the application of DHPG, in most $Cdkl5^{-/y}$ tested neurons (10/14; 71%) we did not observe any effect of DHPG (Fig. 2I). These results disclose novel disrupted mechanisms of excitatory synaptic transmission caused by the absence of CDKL5, selectively involving metabotropic receptors signaling.

2.3 CDPPB potentiates NMDAR current in cortical neurons lacking CDKL5.

It has been shown that when mGluR5 are non-responding to DHPG, their activity can instead be elicited by selective PAMs (Auerbach et al., 2011; Vicidomini et al., 2017). Among these, 3-Cyano-N-(1,3-diphenyl-1H-pyrazol-5-yl)benzamide (CDPPB) offers several advantages compared to agonist drugs such as higher subtype selectivity, reduced desensitization, and more subtle modulatory effects on receptor function (Chen et al., 2008). To start testing this idea in neurons lacking CDKL5, we evaluated CDPPB action on NMDA current. Intriguingly, we found that 2 min application of CDPPB (10 µM) preceding NMDA (50 µM) administration produced a comparable increase of I_{NMDA} (Fig. 2J, lower part) in both genotypes ($Cdkl5^{+/y}$ 42.92%; $Cdkl5^{-/y}$ 45.19%, fig. 2K). Interestingly, most of both $Cdkl5^{-/y}$ and $Cdkl5^{+/y}$ neurons tested showed potentiated I_{NMDA} after the application of CDPPB ($Cdkl5^{+/y}$: 13/18, 78%; $Cdkl5^{-/y}$ 10/12, 83%, fig. 2L) resulting in a significantly higher percentage of $Cdkl5^{-/y}$-neurons responding to CDPPB treatment compared to DHPG (chi-square $Cdkl5^{-/y}$-DHPG: 29% vs $Cdkl5^{-/y}$-CDPPB: 83% $p < 0.0001$). Thus, these results show that mGluR5 stimulation by CDPPB can produce a potent positive effect on NMDA-mediated excitatory synaptic transmission in neurons lacking CDKL5.

Fig.2

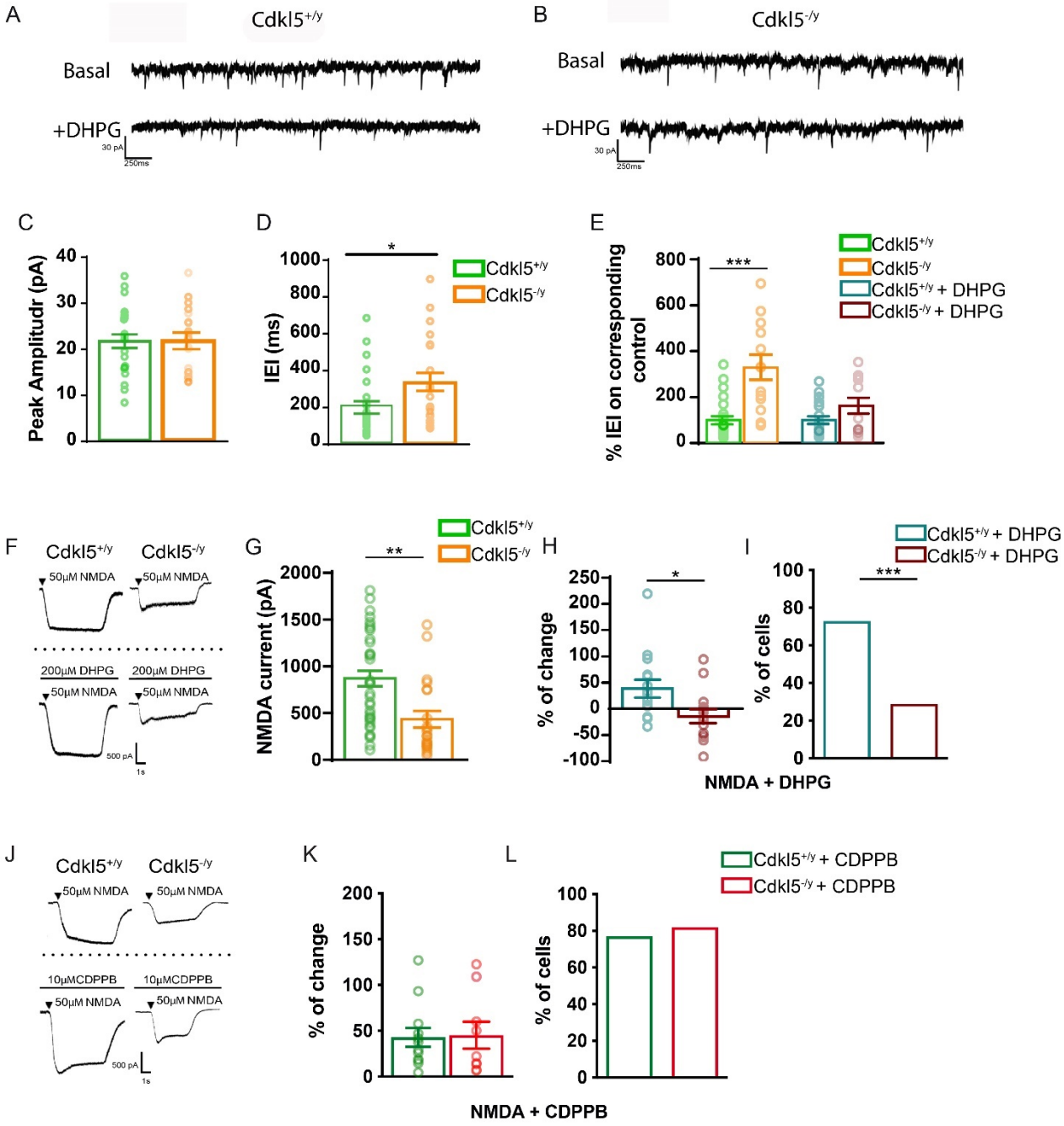

Figure 2. CDKL5 loss tampers with both mEPSCs and mGluR5-induced NMDA current.

*(**A**) Sample traces of miniature excitatory postsynaptic current (mEPSC) recorded from Cdkl5$^{+/y}$ neurons (**A, upper part**) and Cdkl5$^{-/y}$ neurons (**B, upper part**) and after the application of DHPG (**A, B lower part**). (**C-D**) Histograms showing the mean average amplitude (**C**) and the inter-event interval (IEI) of mEPSCs (**D**). (**E**) Histograms displaying the % change of IEI after the application of DHPG (100 μM). (**F**) Representative traces of currents obtained with patch-clamp recordings on*

*S1 neurons cultures from Cdkl5$^{+/y}$ and Cdkl5$^{-/y}$ embryos after NMDA (50 µM) application (**upper part**), and after 2-min application of DHPG (100 µM) + NMDA (**F, lower part**). (**G**) Histograms showing differences of I_{NMDA} current between genotypes. (**H**) Histograms showing the % change of I_{NMDA} after the application of DHPG. (**I**) Histograms displaying the percentage of cells showing potentiated I_{NMDA} after the application of DHPG. (**J**). Representative traces of recorded S1 neuron cultures after NMDA application (**upper part**) and 2-min CDPPB + NMDA application (**lower part**). (**K**) Histograms showing the % change of I_{NMDA} current after the application of CDPPB. (**L**) Histograms displaying the % of cells showing potentiated I_{NMDA} after the application of CDPPB. Student's t-test, chi-square, two-way ANOVA followed by Fisher's multiple comparison test, * p < 0.05, ** p < 0.01, *** p < 0.001 (mEPSC Cdkl5$^{+/y}$ n = 22 cells, Cdkl5$^{-/y}$ n = 28; minis+DHPG: n = 12 cells. NMDA: Cdkl5$^{+/y}$ n = 36 cells, Cdkl5$^{-/y}$ n = 23 cells; NMDA+DHPG Cdkl5$^{+/y}$ n = 15 cells and NMDA+DHPG Cdkl5$^{-/y}$ n = 14 cells; NMDA+CDPPB Cdkl5$^{+/y}$ n = 12 cells; NMDA+CDPPB Cdkl5$^{-/y}$ n = 9 cells).*

2.4 CDPPB treatment ameliorates visual, sensorimotor and memory functions in Cdkl5$^{-/y}$ mice.

Encouraged by the positive effects that we obtained using CDPPB on synaptic currents, we evaluated the therapeutic potential of this PAM by treating mice with one intraperitoneal injection (i.p.) of CDPPB (3 mg/Kg), as in Vicidomini et al. (2017), and the animals were then exposed to a battery of tests.

We investigated cortical visual responses by transcranial intrinsic optical signal (IOS) imaging before and after CDPPB administration in the same animals. As expected from our previous data (Lupori et al., 2019; Mazziotti et al., 2017) baseline response amplitude of Cdkl5$^{-/y}$ mice was strongly decreased compared to Cdkl5$^{+/y}$ littermates (one way ANOVA $p < 0.01$; Tukey multiple comparison Cdkl5$^{+/y}$ vs CDPPB-Cdkl5$^{-/y}$ $p < 0.01$; Cdkl5$^{+/y}$ vs vehicle-Cdkl5$^{-/y}$ $p < 0.01$; vehicle-Cdkl5$^{-/y}$ vs CDPPB-Cdkl5$^{-/y}$ $p = 0.92$. Fig. 3A, B). After CDPPB treatment, visual responses

approached Cdkl5$^{+/y}$ levels (one way ANOVA $p < 0.01$; Tukey multiple comparison Cdkl5$^{+/y}$ vs CDPPB-Cdkl5$^{-/y}$ post injection $p = 0.6$; Cdkl5$^{+/y}$ vs vehicle-Cdkl5$^{-/y}$ post injection $p < 0.05$) significantly increasing from their baseline values (two-way RM ANOVA; main effects not significant, interaction treatment*time $p < 0.05$; Sidak multiple comparison: vehicle-Cdkl5$^{-/y}$ post injection vs CDPPB-Cdkl5$^{-/y}$ post injection $p < 0.05$; CDPPB-Cdkl5$^{-/y}$ baseline vs CDPPB-Cdkl5$^{-/y}$ post injection $p < 0.05$; vehicle-Cdkl5$^{-/y}$ baseline vs vehicle-Cdkl5$^{-/y}$ post injection $p = 0.90$). By contrast, visual response remained impaired in vehicle-treated mutant mice. These experiments indicate that the cortical visual impairment (CVI) shown by Cdkl5$^{-/y}$ mice can be rescued by CDPPB treatment.

When we assessed sensorimotor responses by using the adhesive tape-removal test (Bouet et al., 2009; Komotar et al., 2007), we found that Cdkl5$^{-/y}$ mice display a significant increase in the time-to-contact the tape compared to Cdkl5$^{+/y}$ mice (vehicle-Cdkl5$^{+/y}$ vs vehicle-Cdkl5$^{-/y}$ $p < 0.01$; fig. 3C). Importantly, a single CDPPB injection produced a reduction of the latency exclusively in mutant mice whose performance became similar to controls (vehicle-Cdkl5$^{+/y}$ vs CDPPB-Cdkl5$^{-/y}$ $p > 0.4$; fig. 3C). Finally, the effect of CDPPB was assessed in the Y-maze paradigm for working memory, a feature known to be impaired in Cdkl5$^{-/y}$ mutants (Fuchs et al., 2014). First, we found that the number of the correct spontaneous alternations is decreased in Cdkl5$^{-/y}$ mice compared to Cdkl5$^{+/y}$ animals (vehicle-Cdkl5$^{+/y}$ vs vehicle-Cdkl5$^{-/y}$ $p < 0.01$; fig. 3D), confirming previous observations. Intriguingly, CDPPB rescued working memory defects in Cdkl5$^{-/y}$ mice by normalizing the frequency of spontaneous alternations (vehicle-Cdkl5$^{+/y}$ vs CDPPB-Cdkl5$^{-/y}$ $p > 0.4$; fig. 3D), without altering the performance of Cdkl5$^{+/y}$ mice. No difference in the total number of arms entries were found between genotypes under either treated or untreated conditions (fig. 3E). Thus, these data indicate that the action of CDPPB can reverse atypical functional responses, such as CVI, and memory deficits shown by Cdkl5$^{-/y}$ mice.

Fig.3

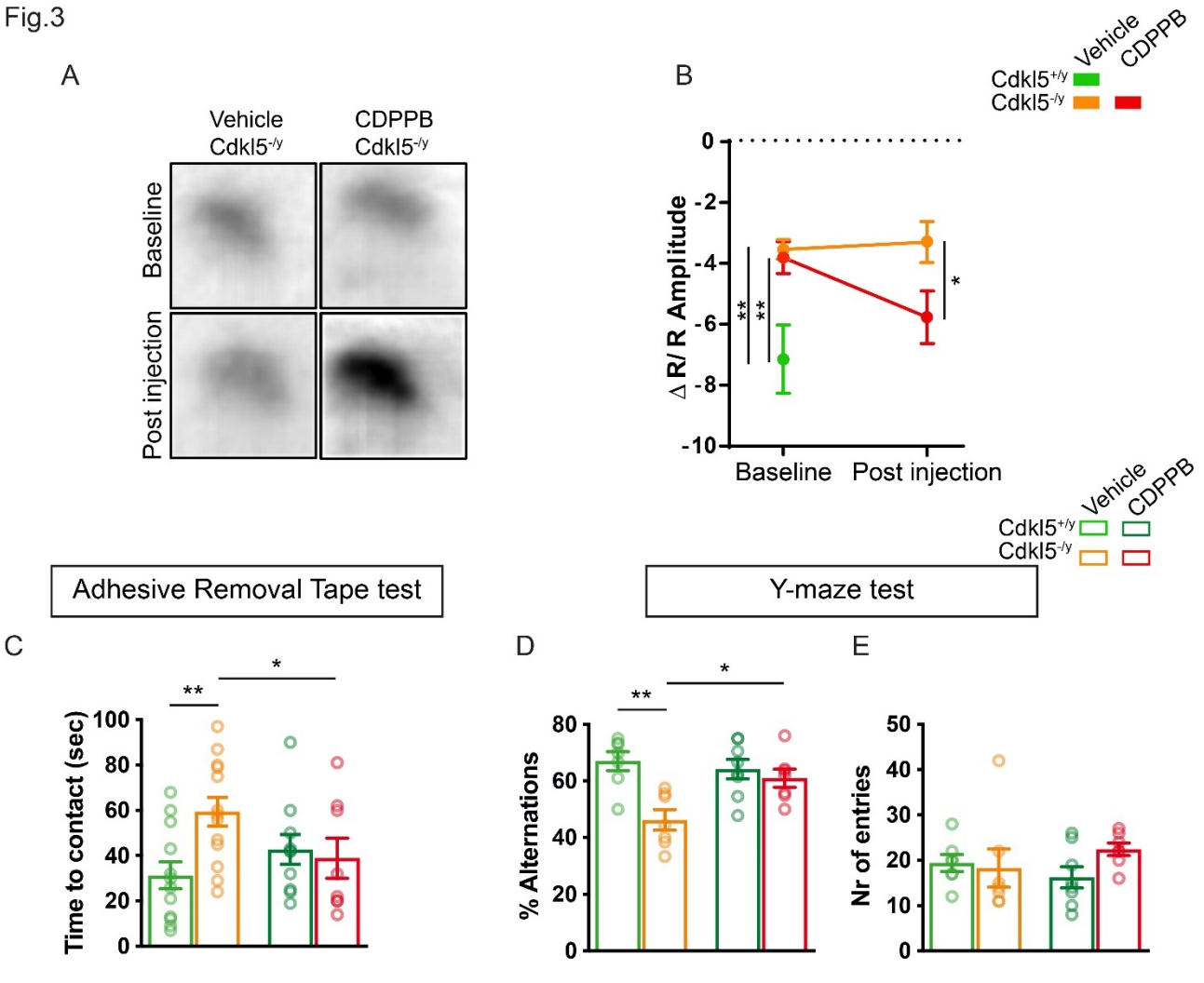

Figure 3. Acute CDPPB treatment rescues CVI, sensorimotor and memory deficits in Cdkl5$^{-/y}$ mice. *(**A**) Samples images showing differences of IOS evoked responses in vehicle- and CDPPB-treated Cdkl5$^{-/y}$ mice. (**B**) Trajectory of the IOS amplitude in vehicle-Cdkl5$^{+/y}$, vehicle-Cdkl5$^{+/y}$ and CDPPB-Cdkl5$^{-/y}$ treated mice. (**C**) Histograms showing contact latency with the tape placed under mice's forepaw. (**D, E**) Histograms showing the percentage of the correct alternations (**D**) and the number of entries (**E**) made by Cdkl5$^{+/y}$ and Cdkl5$^{-/y}$ mice, treated with either vehicle or CDPPB, in the Y-maze. Two-way ANOVA followed by Sidak or Bonferroni's multiple comparison test, * p< 0.05, ** p< 0.01 (IOS: vehicle-Cdkl5$^{+/y}$ n = 3, vehicle-Cdkl5$^{-/y}$ n = 8, CDPPB-Cdkl5$^{-/y}$ n = 6; behavioural tests: vehicle-Cdkl5$^{+/y}$ n = 12, vehicle-Cdkl5$^{-/y}$ n = 13, CDPPB-Cdkl5$^{+/y}$ n = 8, CDPPB-Cdkl5$^{-/y}$ n = 7).*

2.5 mGluR5 PAMs rescue both synaptic and activity defects in Cdkl5$^{-/y}$ cerebral cortex.

In parallel with the observed behavioural and functional rescues, we found that the acute CDPPB treatment produced a normalization of the number and organization of postsynaptic sites as well as of the activity in primary cortices of Cdkl5$^{-/y}$ mice. CDPPB increased the density of Homer1bc^{+} puncta in both S1 and V1 cortices of Cdkl5$^{-/y}$ mice (S1: layers II-III and layer V vehicle-Cdkl5$^{-/y}$ vs CDPPB-Cdkl5$^{-/y}$ $p < 0.01$. V1: layers II-III and layer V vehicle-Cdkl5$^{-/y}$ vs CDPPB-Cdkl5$^{-/y}$ $p < 0.05$; fig. 4A-C), reproducing Cdkl5$^{+/y}$ mice conditions (S1 and V1: layer II-III and layer V: vehicle-Cdkl5$^{+/y}$ vs CDPPB-Cdkl5$^{-/y}$ $p > 0.3$; fig. 4A-C). Intriguingly, CDPPB treatment also established typical mGluR5^{+} puncta density in both S1 and V1 cortices of Cdkl5$^{-/y}$ mice (S1: layers II-III and layer V: vehicle-Cdkl5$^{-/y}$ vs CDPPB-Cdkl5$^{-/y}$ $p < 0.001$; vehicle-Cdkl5$^{+/y}$ vs CDPPB-Cdkl5$^{-/y}$ $p > 0.3$. V1: layers II-III and layer V: vehicle-Cdkl5$^{-/y}$ vs CDPPB-Cdkl5$^{-/y}$ $p < 0.05$. S1 and V1: vehicle-Cdkl5$^{+/y}$ vs CDPPB-Cdkl5$^{-/y}$ $p > 0.3$; fig. 4D-F). Finally, the density of cells expressing ARC, an immediate-early gene induced by mGluR5 activation (Ménard and Quirion, 2012; Wang and Zhuo, 2012), was restored in the V1 cortex of CDKL5-mutants after a single CDPPB administration (layers I-VI: vehicle-Cdkl5$^{+/y}$ vs vehicle-Cdkl5$^{-/y}$ $p < 0.01$; vehicle-Cdkl5$^{-/y}$ vs CDPPB Cdkl5$^{-/y}$ $p < 0.001$; fig. 4G,H).

Fig. 4

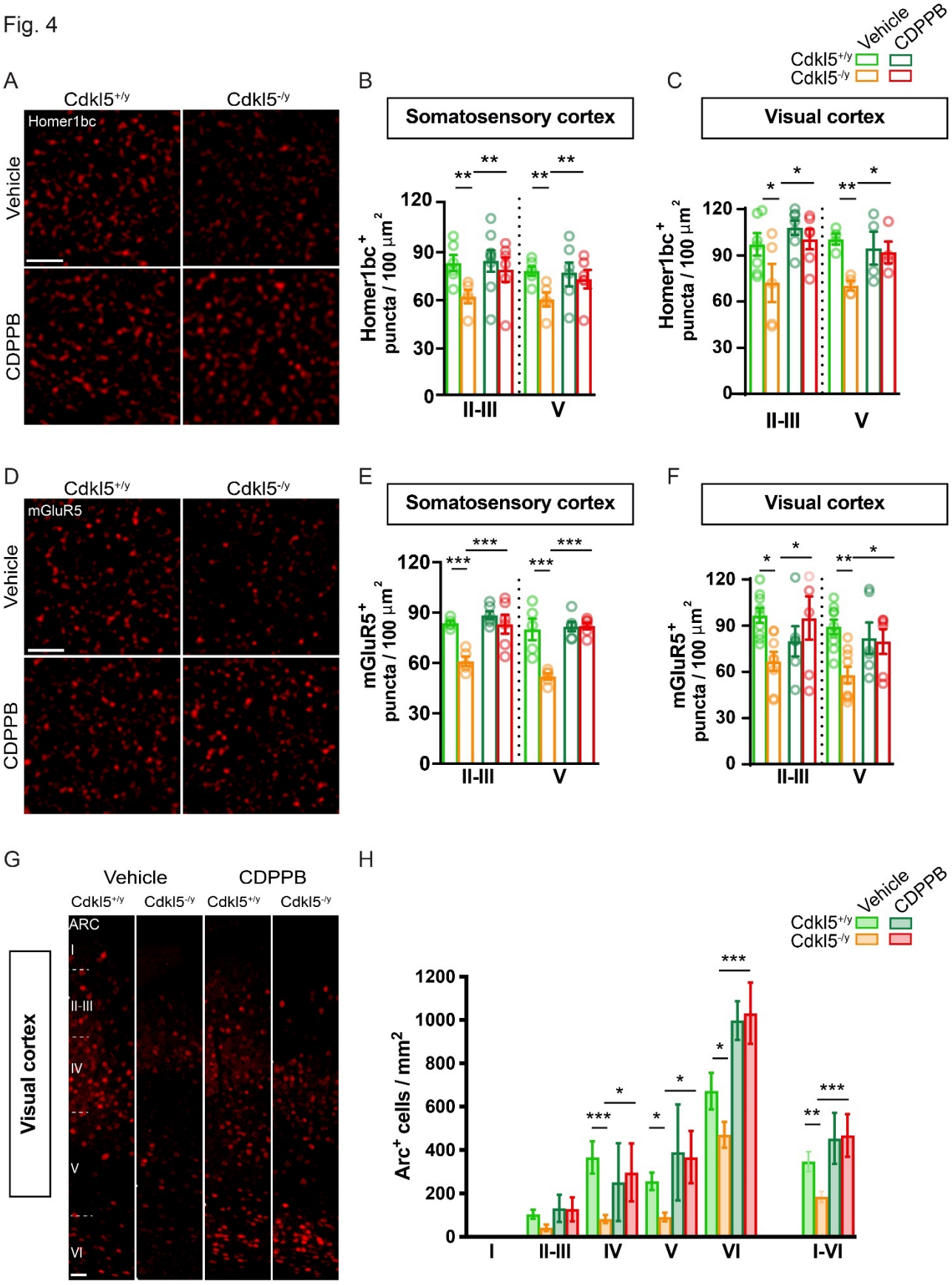
A
Cdkl5+/y
Cdkl5-/y
Homer1bc
Vehicle
CDPPB
B
Somatosensory cortex
Homer1bc+ puncta / 100 µm2
II-III
V
C
Visual cortex
Vehicle
CDPPB
Cdkl5+/y
Cdkl5-/y
D
mGluR5
E
Somatosensory cortex
mGluR5+ puncta / 100 µm2
F
Visual cortex
G
Vehicle
CDPPB
ARC
Visual cortex
I
II-III
IV
V
VI
H
Arc+ cells / mm2
I
II-III
IV
V
VI
I-VI

Figure 4. Structural defects exhibited by Cdkl5$^{-/y}$ mice cortices are rescued by an acute CDPPB injection. *(**A, D**) Representative confocal images showing Homer1bc^{+} and mGluR5^{+} puncta in layer II-III of S1 cortex from either vehicle- or CDPPB-treated mice (scale bar: 5 µm). (**B, C, E, F**) Histograms showing both Homer1bc^{+} (**B, C**) and mGluR5^{+} (**E, F**) immunopuncta density in layers II-III and V of both S1 (**B, E**) and V1 (**C, F**) cortices in either vehicle- or CDPPB-treated mice. (**G**) Confocal images of ARC immunostaining on coronal sections of the V1 cortex from mice treated with vehicle or CDPPB (scale bar: 25 µm), and relative ARC^{+} cells density quantitation (**H**) throughout the cortical layers. Two-way ANOVA followed by Fisher's multiple comparison test, *p < 0.05, ** p < 0.01, *** p < 0.001; (n = 6 animals for each genotype).*

In order to increase the reproducibility of our study, we treated another group of Cdkl5$^{-/y}$ and Cdkl5$^{+/y}$ animals with a different mGluR5 PAM, the RO6807794 (RO68) compound (Kelly et al., 2018). Two hours after an i.p. injection with RO68 (0.3 mg/kg), we found that the density of Homer1bc^{+} puncta in S1 cortex of Cdkl5$^{-/y}$ mice was increased (S1: layers II-III and layer V vehicle-Cdkl5$^{-/y}$ vs CDPPB-Cdkl5$^{-/y}$ $p < 0.05$. V1: layers II-III and layer V vehicle-Cdkl5$^{-/y}$ vs CDPPB-Cdkl5$^{-/y}$ $p < 0.05$; fig. S1 A-B) to reproduce Cdkl5$^{+/y}$ mice conditions (S1 layer II-III and layer V: vehicle-Cdkl5$^{+/y}$ vs CDPPB-Cdkl5$^{-/y}$ $p > 0.3$; fig. S1A-B). Intriguingly, RO68 was also able to restore the activation levels of S1 cortex in Cdkl5$^{-/y}$ mice (Fig. S1 C) throughout cortical layers (vehicle-Cdkl5$^{+/y}$ vs vehicle-Cdkl5$^{-/y}$ $p < 0.001$; vehicle-Cdkl5$^{-/y}$ vs RO68-Cdkl5$^{-/y}$ $p < 0.001$), as indicated by the c-Fos^{+} cell density count (Fig. S1 D; see also Pizzo et al., 2016), that reached the magnitude of Cdkl5$^{+/y}$ mice (vehicle Cdkl5$^{+/y}$ vs CDPPB-Cdkl5$^{-/y}$ $p > 0.05$). These results strongly support the idea that mGluR5-mediated signaling represents an effective therapeutic target for reverting neurological signs in CDD.

2.6 The effects of a protracted CDPPB treatment in Cdkl5$^{-/y}$ mice are long-lasting.

To assess the therapeutic potential of mGluR5 modulation, we treated animals for five consecutive days with CDPPB and 24 hours after the last injection animals were behaviourally tested and then sacrificed for brain analyses. We found that after this protracted treatment, the density of Homer1bc^{+} puncta remained increased in both upper and deeper layers of the S1 cortex in mutant mice (layers II-III and layer V: vehicle-Cdkl5$^{-/y}$ vs CDPPB-Cdkl5$^{-/y}$ $p < 0.01$; fig. 5A, B), and that its value was no different from Cdkl5$^{+/y}$ levels (layers II-III and layer V: vehicle-Cdkl5$^{+/y}$ vs CDPPB-Cdkl5$^{-/y}$ $p > 0.3$; fig. 6B). In contrast, no effect of CDPPB on Homer1bc expression was found in Cdkl5$^{+/y}$ animals (layers II-III and layer V: vehicle-Cdkl5$^{+/y}$ vs CDPPB-Cdkl5$^{+/y}$ $p > 0.9$; fig. 5A, B). Next, we analysed hind-limb clasping, one solid sign shown by Cdkl5$^{-/y}$ mice (Amendola et al., 2014; Terzic et al., 2021; Trazzi et al., 2018). In line with previous studies, vehicle-treated mutants showed increased hind-limb clasping compared to Cdkl5$^{+/y}$ littermates (vehicle-Cdkl5$^{+/y}$ vs vehicle-Cdkl5$^{-/y}$ $p < 0.001$; fig. 5C -Amendola et al., 2014) whereas after CDPPB treatment Cdkl5$^{-/y}$ mice spent significantly less time clasping their hind paws (vehicle-Cdkl5$^{-/y}$ vs CDPPB-Cdkl5$^{-/y}$ $p < 0.01$; fig. 5C). Nevertheless, clasping time was significantly higher in treated mutants compared to Cdkl5$^{+/y}$ mice (vehicle-Cdkl5$^{+/y}$ vs. CDPPB-Cdkl5$^{-/y}$ $p < 0.01$; fig. 5C). Finally, we evaluated the effects of sub-chronic CDPPB treatment on cortical activity by analysing c-Fos expression. Although there was only a small increase, not statistically significant, of c-Fos expression in treated-mutant mice (vehicle-Cdkl5$^{+/y}$ vs vehicle-Cdkl5$^{-/y}$ $p < 0.01$; vehicle-Cdkl5$^{-/y}$ vs CDPPB-Cdkl5$^{-/y}$ $p = 0.09$; fig. 5 D, E;), c-Fos levels were no longer different between genotypes after CDPPB treatment (vehicle Cdkl5$^{+/y}$ vs CDPPB-Cdkl5$^{-/y}$ $p > 0.09$; fig. 5E). Taken together, these data indicate that protracted CDPPB treatment is accompanied by long-lasting positive effects in Cdkl5$^{-/y}$ mice, a result consistent with the design of a therapeutic protocol for CDD targeting mGluR5.

Fig. 5

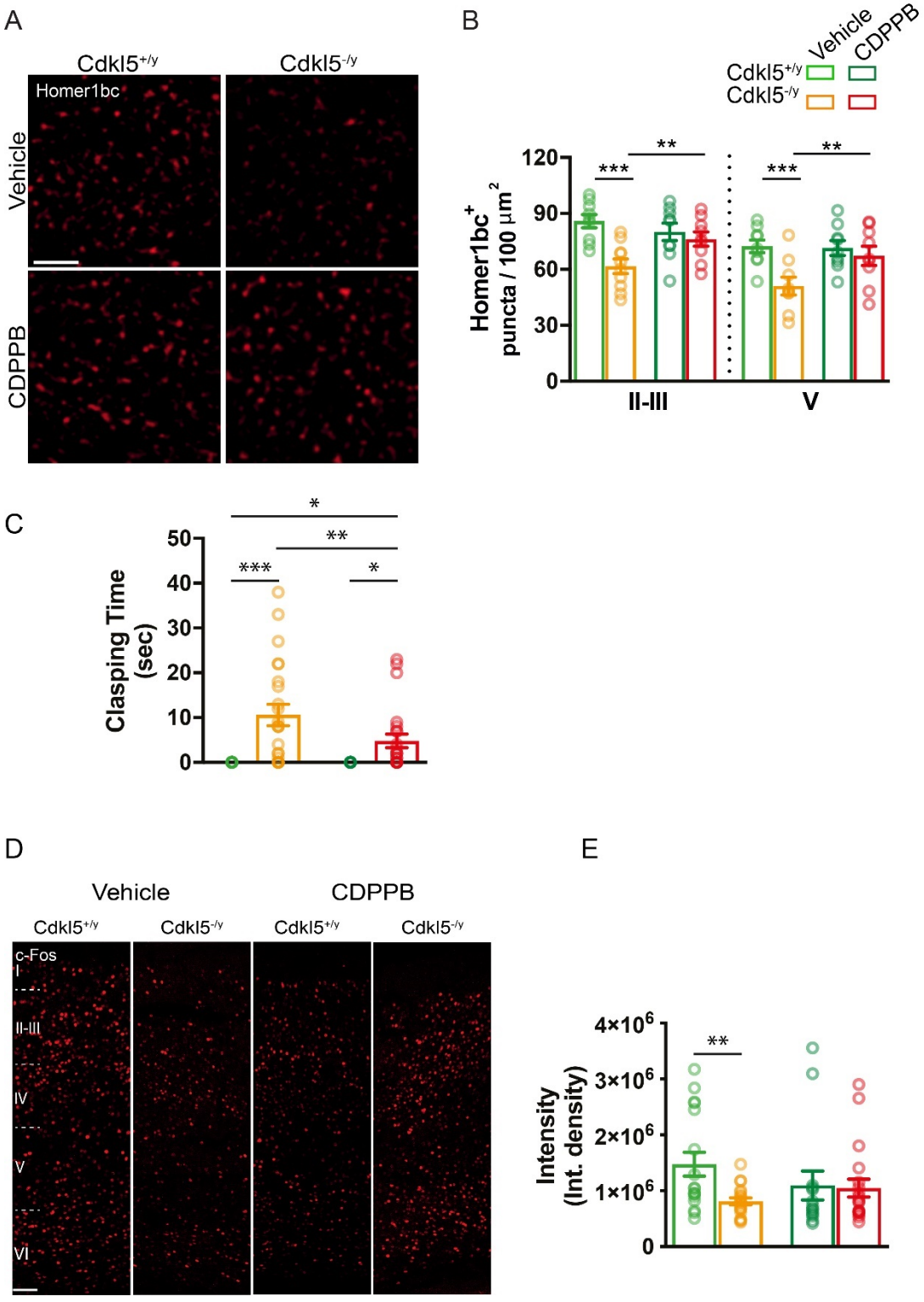

Figure 5. The subchronic treatment with CDPPB produces lasting effects in Cdkl5$^{-/y}$ mice.

*(**A**) Representative confocal images of Homer1bc^{+} (red) immunofluorescence in layers II-III of the S1 cortex. (**B**) Histograms showing Homer1bc^{+} puncta density in layers II-III and V of the S1 cortex*

*of either vehicle- or CDPPB-treated mice. (**C**) Histograms showing time spent clasping in vehicle- or CDPPB-treated mice. (**D**) Representative images of c-Fos immunoreactive cells in S1 of vehicle- or CDPPB-treated mice (scale bar 50 µm). (**E**) Histograms showing the integrated intensity analysis of c-Fos immunofluorescence in the S1 of vehicle- or CDPPB-treated mice. Two-way ANOVA followed by Fisher's LSD: * $p < 0.05$, ** $p < 0.01$, *** $p < 0.001$ (Homer1bc$^+$ puncta: n = 9 for each group; clasping and c-Fos vehicle-Cdkl5$^{+/y}$ n = 34, vehicle-Cdkl5$^{-/y}$ n = 23, CDPPB-Cdkl5$^{+/y}$ n = 17, CDPPB-Cdkl5$^{-/y}$ n = 23).*

2.7 The BA17 cortex of CDD patients recapitulates the mGlur5 defects shown by Cdkl5$^{-/y}$ mice.

Finally, to look into the translational potential of our findings, we examined excitatory synaptic structures in the 2 postmortem CDD patient brains available worldwide that we obtained from the Harvard Brain Tissue Resource Center (Belmont; USA). These experiments were performed on sections from the primary visual cortex (BA17) of CDD cases and age/sex-matched neurotypical subjects (NTs). Intriguingly, the results showed a clear reduction of both postsynaptic proteins PSD-95$^+$ and Homer1bc$^+$ as well as of the presynaptic marker VGluT1$^+$, irrespective of case age (5 and 30 years old), compared to NTs (fig. 6A, D). Moreover, although a statistical analysis was not performed with only 2 cases, the quantification of the immunopuncta revealed a reduction in the cortices of CDD patients compared to NTs (fig. 6A-E), indicative of an overall reduction of glutamatergic synapses. We next evaluated Homer1bc, PDS-95 and mGluR5 expression by western blotting on BA17 cortex lysates. Intriguingly, as shown in figures 6 F-I, the BA17 area from CDD samples showed a robust reduction in the expression of these synaptic proteins compared to NTs. Although derived from a limited dataset, these results suggest that structural features of CDD largely overlap between mice and human cortices and are supportive of the clinical potential for a mGluR5-directed therapeutic strategy.

Fig. 6

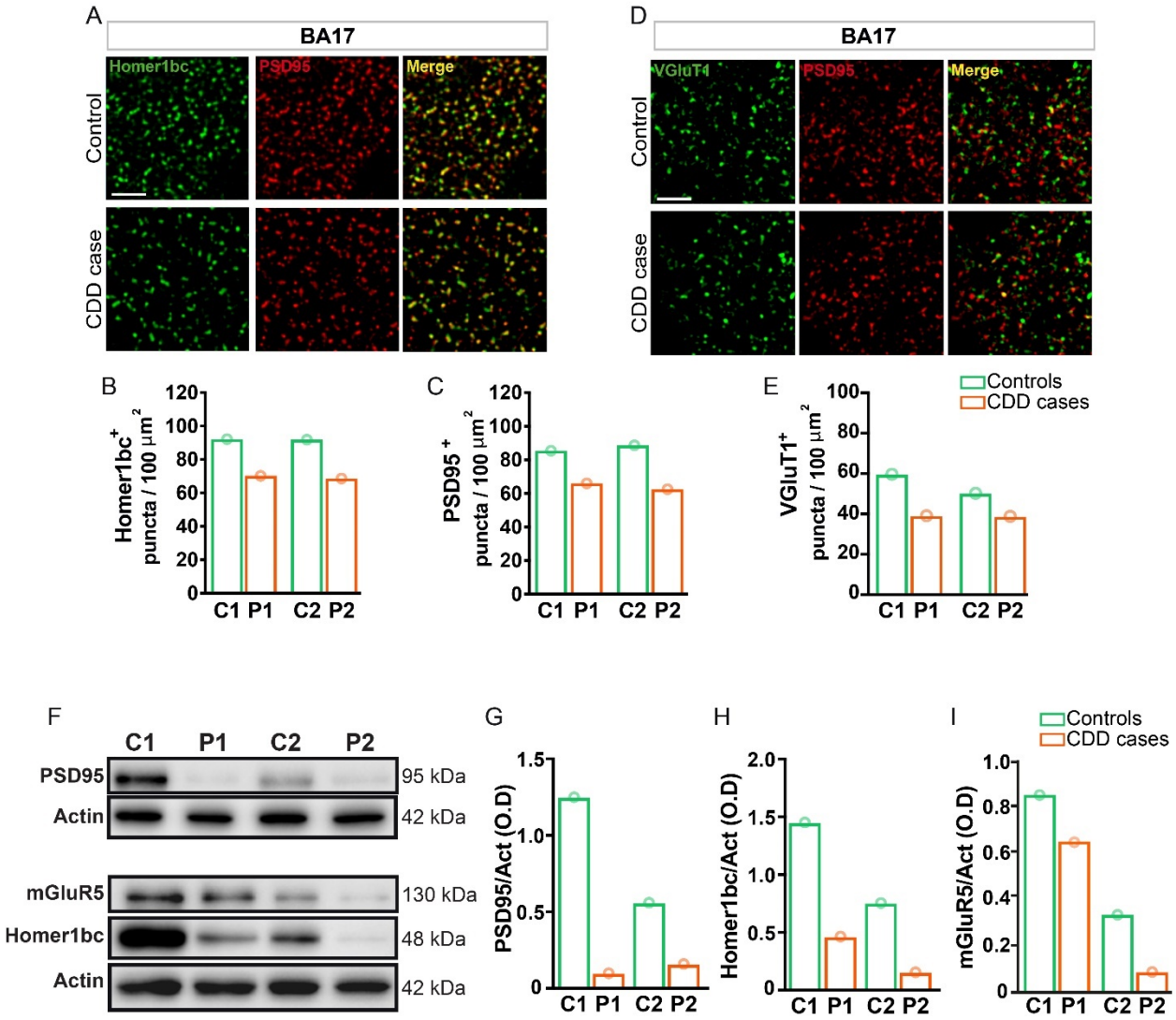

Figure 6. Aberrant expression of excitatory synaptic proteins in the BA17 cortex of CDD patients. *(**A, D**) Illustrative confocal images taken from layers II-III of the BA17 cortex. (**A**) PSD-95^{+}(red), Homer1bc^{+}(green), (**D**) VGluT1^{+}(green) immunofluorescence puncta. Note the virtually complete overlapping of PSD-95 and Homer1bc immunofluorescence (scale bar: 5 µm). (**B, C, E**) Histograms showing the analysis of puncta density in layers II-III of BA17 cortices. (**F**) Western blotting showing the expression of PSD95, Homer1bc and mGluR5 in lysates from BA17 cortices. (**G**) Histograms displaying the optical density (O.D.) analysis of PSD95, Homer1bc and mGluR5 expression. Student's t-test, * $p < 0.05$, ** $p < 0.01$ (C1 = F, 4 years old; P1 = F, 5.7 years old; C2 = F, 29 years old; P2 = F, 30 years old).*

3. Discussion

It is urgent to find therapeutic targets and treatments for CDD, a devastating condition without any corrective option. In this study, we focus our attention on mGluR5, a metabotropic glutamate receptor highly expressed in the cerebral cortex which activity requires the binding with Homer1bc (Aloisi et al., 2017), a scaffolding protein that is severely downregulated in the cerebral cortex of both CDKL5$^{-/y}$ mice and CDD patients (Pizzo et al., 2019, 2016; fig. 6A,B) as well as in iPSCs-derived neurons from CDD patients (Negraes et al., 2021). Interestingly, we show for the first time that CDKL5 plays a role in the formation of mGluR5-Homer1bc complexes at synapses because both the localization of mGluR5 and its binding with Homer1bc are defective in the S1 cortex of CDKL5 mutant mice. Also, we show here that the function of GluR5 at excitatory synapses is faulty in neurons lacking CDKL5. We find that synaptic transmission, both basal and NMDA-mediated, is altered in S1 neurons lacking CDKL5 and that it is unresponsive to the modulation normally produced by the selective mGluR5 agonist DHPG. Because Shank1, by forming complexes with Homer1bc, PSD-95 and NMDAR, promotes the cooperation between NMDAR and mGluR5 signaling machineries (Ango et al., 2000; Hering and Sheng, 2001; Tu et al., 1999), our results are the first to suggest that lack of CDKL5 tampers with the synergistic cooperation between these glutamatergic receptors. This effect is likely produced by a reduced amount of Homer1bc recruited in the postsynaptic density in the absence of CDKL5 which, in turn, results in an atypical postsynaptic localization/stabilization of mGluR5. Interestingly, aberrant NMDA receptors signaling have been previously reported by Okuda and colleagues (2017) in the hippocampus of a different CDKL5 mutant mice line showing severe NMDA-dependent epileptic seizures due to the incorrect postsynaptic accumulation of GluN2B-containing NMDA receptors (Okuda et al., 2017). Similar results have been obtained in the hippocampus of the Cdkl5^{R59X} knock-in CDD mouse model (Yennawar et al., 2019). Altogether, although with some differences, these findings further support the idea that CDKL5 plays a crucial role in the correct localization/function of glutamate receptors, both ionotropic and metabotropic, at the synapse.

Remarkably, an aberrant expression and function of mGluR5 has been reported in several neurodevelopmental diseases such as Fragile X, Phelan McDermid syndrome, Tuberous sclerosis (TSC) and Rett syndrome (Aloisi et al., 2017; Auerbach et al., 2011; Gogliotti et al., 2016; Vicidomini et al., 2017) pointing to mGluR5 signaling defects as a shared feature among genetic forms of neurodevelopmental disorders. The reduced expression/function of mGluR5, combined with relevant synaptic and behavioural signs shown by CDKL5 mutant mice, provided us with solid bases for attempting the first preclinical assessment of mGluR5 PAMs efficiency for CDD that we report in this study. Intriguingly, our results revealed that an acute treatment with CDPPB is effective in restoring several endophenotypes and behavioural signs produced by CDKL5 loss both *in-vitro* and *in-vivo*. Our data show that in primary cortical neuronal cultures, CDPPB can restore mGluR5-mediated potentiation of NMDA currents in CDKL5$^{-/y}$ pyramidal neurons. Considering the negative response of NMDA current to DHPG treatment that we report in mutant neurons, the effect of CDPPB is surprising although closely replicating what has been found previously in Shank3-KO neurons (Vicidomini et al., 2017). These results further support the possibility that the pharmacological action of CDPPB also results from a residual agonist-like activity that has been previously documented (Kinney et al., 2005; Vicidomini et al., 2017). Furthermore, the present findings strongly suggest that CDPPB treatment can facilitate the functional maturation of dendritic spines in the absence of CDKL5, as it increases the synaptic expression of both Homer1bc and mGluR5, two crucial molecular determinants of spine formation and stabilization (Oh et al., 2013; Sala et al., 2003). These synaptic effects are reflected by beneficial outcomes at the functional and behavioural level in mutant animals that are mostly relevant in the context of CDD. Our data, showing for the first time that CVI and overall cortical activity in CDKL5$^{-/y}$ mice can be rescued by CDPPB treatment, strengthens the translational value of our preclinical results. As a matter of fact, recent data indicate that CVI is correlated with reduced milestone achievement in CDD patients and therefore CVI can be used in the clinic as a solid biomarker for CDD diagnosis, progression, and treatment with biunivocal translational validity (Demarest et al., 2019; Lupori et al., 2019).

Interestingly, our findings indicate that mGluR5 signaling greatly suffers from the lack of CDKL5, but it does not become completely non-functional. As a matter of fact, the protracted treatment with CDPPB in CDKL5-null mice reveals that the rescuing effect on both the density of dendritic spine-like structures and cortical c-Fos expression in the cerebral cortex as well as the amelioration of the hindlimb-clasping phenotype is long-lasting. Thus, although further studies are needed to dissect out the mechanisms of CDPPB action on excitatory synapse signaling, our results encourage further testing of mGluR5 PAMs in animals modelling CDD and offer hope for a future use of these compounds in the clinic. In line with this idea, our set of data obtained with another mGluR5 PAM, the RO68 compound, strengthen the role of mGluR5 as novel druggable targets for CDKL5 deficiency. Considerably, RO68 has the clinically relevant advantage that it can be dissolved in salina with an extremely low percentage of detergent (i.e.: Tween-80) and has a higher potency compared to other mGluR5 PAMs. Remarkably, RO68 is efficacious even at very low concentrations (i.e.: 0.3 mg/kg), thus reducing the risk of toxicity, as we show in this study where this compound was able to rescue neuroanatomical, functional and behavioural signs of CDKL5 mutant mice, and as it was previously shown in a mouse model of TSC (Kelly et al., 2018). Finally, the positive action of mGluR5 PAMs on the molecular organization of postsynaptic structures is even more exciting in view of our analyses on the two post-mortem CDD brains available. Our data strongly suggest that synaptic abnormalities and mGluR5 downregulation are signs that occur also in human patients, and that are potentially rescuable by positive allosteric modulation of mGluR5.

To sum up, we believe that these data on the efficacy of mGluR5 activation pave the way for including these receptors as a promising therapeutic target for CDD. Our results also suggest that an early-onset and prolonged regime of mGluR5 activation has the potential to stably revert the mophofunctional defects shown by adult CDKL5 mutants. Finally, this study further supports previous indications that abnormalities of mGluR5 signaling represents a solid hallmark for multiple neurodevelopmental diseases, now including CDD.

4. Materials and Methods

Animals and pharmacological treatment

Animal care and handling throughout the experimental procedures were conducted in accordance with European Community Council Directive 2010/63/UE for care and use of experimental animals with protocols approved by the Italian Minister for Scientific Research (Authorization number 38/2020-PR) and the Bioethics Committee of the University of Torino, Italy. Animal suffering was minimized, as was the number of animals used. Mice for testing were produced by crossing Cdkl5$^{-/x}$ females with Cdkl5$^{-/y}$ males or with Cdkl5$^{+/y}$ males. Littermate controls were used for all the experiments. After weaning, mice were housed 4 per cage on a 12 h light/dark cycle (lights on at 7:00 h) in a temperature-controlled environment (21 ± 2◦C) with food and water provided ad libitum. For this study, 8-weeks old (post-natal day 56) Cdkl5$^{-/y}$ and Cdkl5$^{+/y}$ males were used. Because we did not observe any noticeable interindividual phenotypic or metabolic (e.g. weight and health condition scores) difference among the mouse cohorts used in this study, no inclusion/exclusion criteria were adopted besides age (PND56) and sex (male) of the animals. In pharmacological rescue experiments, animals were treated with the selective positive allosteric modulator (PAM) of mGluR5 3-cyano-N-(1,3-diphenyl-1H-pyrazol-5-yl)benzamide (CDPPB; Tocris, UK) that was diluted in saline solution containing 5-10% final concentration of DMSO and polyethylene glycol 400 (DMSO: PEG 400 = 1:9) 5,23. Acutely treated mice received an intraperitoneal injection (ip) of either CDPPB (3 mg/kg) or vehicle 5 at 9.00 am and then put back in their home cage for 1 hour before being behaviourally tested. For sub-chronic administration, animals were treated for five consecutive days and, 24 hours after the last injection, tested. All mice were subsequently sacrificed for brain analyses.

Synaptosomal fraction preparation

Adult mice (PND 56) were killed by decapitation, the entire cortex was rapidly removed and tissue was processed as in 61,62. The tissues were homogenized in ice-cold lysis buffer (0.32 M sucrose, and HEPES 1X at pH 7.4 and 1 mM EGTA, 1mM Na-Orthovanadate, 1 mM DTT, phenylmethylsulphonyl fluoride and 1 mM sodium fluoride and protease inhibitors (SIGMAFAST™ Protease Inhibitor Cocktail Tablets, EDTA-Free), using a glass Teflon tissue grinder. The homogenates were centrifuged at 1000 g for 10 min at 4°C. After discarding the nuclear pellet, the supernatant was centrifuged at 12,500 g for 20 min at 4°C. The P1 fraction was then washed with the same initial volume of lysis buffer and underwent further spin (20 min; 12,500 g). The pellet obtained was the crude cortical synaptosomal fraction (P2) that was resuspended in 400 µl of RIPA buffer (NP-40 1%, Na deoxycholate 0,25%, EDTA 0.5M, NaCl 5M, Tris pH8 1M, SDS 10%) and stored at -80°C. Protein concentration of the synaptosomal fraction was determined with the Bio-Rad protein assay kit (Alfieri et al., 2017).

Co-immunoprecipitation assay

50 µg of proteins from the crude synaptosomal (P2) fractions were incubated for 1 hour at 4 °C in RIA buffer (200 mM NaCl, 10 mM EDTA, 10 mM Na2HPO4, 0.5% Nonidet P-40 supplemented with 0.1% SDS) and protein A/G-agarose beads (Santa Cruz, Dallas, TX, USA) as pre-cleaning procedure. The beads were then let to sediment at the bottom of the tube and the supernatant was collected. Primary antibody (Homer1bc) was added to the supernatant before leaving to incubate overnight (O/N) at 4 °C on a rotating wheel, then protein A/G-agarose beads were added and incubation continued for 2h at RT. Beads were then collected by gravity and washed three times with RIA buffer before adding sample buffer for SDS–polyacrylamide gel electrophoresis (SDS–PAGE) and heating the mix al 95°C for 10 min. Beads were pelleted by centrifugation an

supernatants were separated using 4–15% SDS–PAGE precast gels (Biorad, Italy) (Mellone et al., 2015).

Western blotting

The lysates both immunoprecipitates and the inputs (50% of the total P2 lysates) were boiled in SDS sample buffer, separated by SDS–PAGE and the proteins were then blotted to PVDF membrane following a standard protocol (Grasso et al., 2017). Next, PVDF membranes were blocked in BSA 5% for 1h and incubated with the primary antibodies (see table2) O/N at 4°C. After washes with TBS 0.1% Tween 20, the membranes were incubated with the appropriate secondary antibodies (anti-mouse or anti-rabbit, 1:5000; Sigma, Italy) for 1h at RT. The chemiluminescent signal was visualized using Clarity™ Western ECL Blotting Substrates (Bio- Rad; Italy) and acquired with Bio-Rad ChemiDocTM Imagers (Bio-Rad; Italy) and analysed with Image J software (NIH, Usa).

Human postmortem brain tissue

The CDKL5 specimens were from the Harvard Brain Tissue Resource Center, Belmont (USA). Case P1 was a 5.7-year-old female with a frameshift mutation (c.2153_2154dupTG) in exon 15 of CDKL5 gene that results in a premature stop codon. Case P2 was a 30-year-old female with a deletion of exons 1-3 in CDKL5 gene. Control samples were obtained from the University of Maryland, Baltimore. Case C1 was a 4 years old female whereas case C2 was a 29 years old female. The sections analysed are from the BA17 occipital region of human cerebral cortex.

Immunofluorescence procedures

Cerebral cortical tissue: for synaptic proteins detection, mice were anesthetized using a mix of tiletamine/zolazepam (40mg/kg) and xilazine (4-5 mg/kg) and then decapitated 20. The brains were rapidly excised and manually cut in coronal slabs that were fixed by immersion in ice-cold

paraformaldehyde (4% in 0.1M phosphate buffer, PB, pH 7.4) for 30 min. After fixation, tissue slabs were rinsed in PB 0.1M, cryoprotected by immersion in sucrose-PB 0.1M solutions (10, 20 and 30%), cut in 20-µm sections with a cryostat, mounted on gelatine-coated slides and stored at −20°C until immunolabeling was performed as in 20. For c-Fos, ARC and Homer1bc immunodetection after CDPPB subchronic treatment, animals were anesthetized tiletamine/zolazepam (40mg/kg) and xilazine (4-5 mg/kg) and transcardially perfused with about 10 ml of 0.1M PBS followed by 80 ml of ice-cold 4% paraformaldehyde in 0.1M PB. After the brains were dissected, they were kept in the same fixative solution O/N at 4°C, cryoprotected by immersion in raising sucrose-PB 0.1M solutions (10, 20 and 30%), cut into 30 µm sections with a cryostat and stored at −20°C in a cryoprotectant solution containing 30% ethylene glycol and 25% glycerol until use. Cryosections were subsequently processed free-floating by immersion in 0.1M PBS solution containing 3% normal donkey serum (NDS) and 0.5% Triton X for 1h followed by an O/N incubation at 4°C with the primary antibodies (see table2). The following day the sections were rinsed with 0.1M PBS and incubated with the appropriate fluorescent secondary antibodies (anti-mouse or anti-rabbit 1:1000; Jackson ImmunoResearch, West Grove, PA, USA) for 1h at RT. The sections were washed three times with PBS, mounted on gelatine-coated glass slides and cover slipped with Dako fluorescence mounting medium (Dako Italia, Italy).

Human postmortem brain tissue: for Homer1bc and PSD-95 detection, we performed immunofluorescence on flash-frozen sections. Serial sections (20 µm) were cut by using a cryostat, mounted on superfrost slides and stored at −80°C until immunolabeling was performed. Before starting the immunofluorescence, sections were fixed in cold methanol for 1 min. The sections were then processed for double immunofluorescence by using in combination anti-Homer1bc and anti-PSD-95 primary antibodies and the appropriate fluorescent secondary antibodies (anti-mouse or anti-rabbit 1:1000; Jackson ImmunoResearch, West Grove, PA, USA) following the same protocol used for mouse brain tissue (see Pizzo et al., 2016).

Images acquisition and analysis

All analyses were carried out by an investigator who was blinded to the animal's genotype or treatment as well as to plasmids transfection in cells. For brain sections analyses, the layers of the primary somatosensory and visual (S1 and V1) cortices were identified as previously reported 24,25. Synaptic immunofluorescence puncta, for both mouse and human brain tissue, were analysed on 5 serial optical sections (0.5 μm Z-step size) acquired from layers 2-3 and 5 of S1 and V1 with a laser scanning confocal microscope (LSM5 Pascal; Zeiss, DE) using a 100× oil objective (1.4 numerical aperture) and the pinhole set at 1 Airy unit. The density of the immunopositive puncta was determined by manual count followed by density analysis (puncta/100 μm^2) with Imaris (Bitplane, Zurich, CH) and Image J (USA) softwares. Synaptic puncta were included if present in at least two consecutive optical sections.

For ARC and c-Fos immunofluorescence analyses, confocal images of the mouse S1 and V1 cortices were acquired in at least three corresponding coronal brain sections from at least six animals per group with a 20× objective using a 1-μm Z-step. Digital boxes spanning from the pial surface to the corpus callosum were superimposed at matched locations on each coronal section of V1 and divided into 10 equally sized sampling areas (bins; layer I: bin 1; layer II/III: bins 2–3; layer IV: bins 4–5; layer V: bins 6–7; layer VI: bins 8–10) as in (Tomassy et al., 2014). The density of ARC^+ cells was determined by manual count in each bin using Image J software and expressed as cells/mm2, while intensity values of c-Fos^+ cells were obtained using a dedicated Image J tool (integrative density) to analyse Z-stack projected images (Sum value).

Chronic IOS Imaging

Surgery: for chronic IOS preparations, adult mice were anesthetized and maintained with isoflurane (respectively 3 and 1%), placed on a stereotaxic frame and head fixed using ear bars. Body temperature was controlled using a heating pad and a rectal probe to maintain the animals' body at 37ºC. Local anaesthesia was provided using subcutaneous lidocaine (2%) injection and eyes were protected with dexamethasone-based ointment (Tobradex, Alcon Novartis). The scalp was removed, and the skull carefully cleaned with saline. Skin was secured to the skull using cyanoacrylate. Then a thin layer of cyanoacrylate is poured over the exposed skull to attach a custom-made metal ring (9 mm internal diameter) centred over the binocular visual cortex. When the glue dried off, a drop of transparent nail polish was spread over the area to ameliorate optical access. After surgery the animals were placed in a heated box and monitored to ensure the absence of any sign of discomfort. Before any other experimental procedure, mice were left to recover for 24/48h. During this period, paracetamol (5 mg/ml) was administered in the water as antalgic therapy.

Visual stimulation, data acquisition and analysis: IOS recordings were performed under Isoflurane (1%) and Chlorprothixene (1.25mg/Kg, i.p.). Images were visualized using an Olympus microscope (BX50WI). Red light illumination was provided by 8 red LEDs (625 nm, Knight Lites KSB1385-1P) attached to the objective (Zeiss Plan-NEOFLUAR 5x, NA: 0.16) using a custom-made metal LED holder. The animal was secured under the objective using a ring-shaped neodynium magnet (www.supermagnete.it, R-12-09-1.5-N) mounted on an arduino-based 3D printed imaging chamber that also controls eye shutters and a thermostated heating pad. Visual stimuli were generated using Matlab Psychtoolbox and presented on a gamma corrected 9.7-inch monitor, placed 10 cm away from the eyes of the mouse. Sine wave gratings were presented in the binocular portion of the visual field (-10º to +10º relative to the horizontal midline and -5º to +50º relative to the vertical midline) with a spatial frequency of 0.03 cycles per degree, mean luminance 20 cd/m2 and a contrast of 90%. The stimulus consisted in the abrupt contrast reversal of a grating with a temporal frequency of 4

Hz for 1 sec, time locked with a 16-bit depth acquisition camera (Hamamatsu digital camera C11440) using a parallel port trigger. Interstimulus time was 14 sec. Frames were acquired at 30 fps, with a resolution of 512 x 512 pixels. A total of 270 frames were captured for each trial: 30 before the stimulus as a baseline condition and 240 as post-stimulus. The signal was averaged for at least 30 trials and downsampled to 10 fps. Fluctuations of reflectance (R) for each pixel were computed as the normalized difference from the average baseline (ΔR/R). For each recording, an image representing the mean evoked response was computed by averaging frames between 0.5 to 2.5 sec after stimulation. The mean image was then low-pass filtered with a 2D average spatial filter (30 pixels, 117 μm2 square kernel). To select the binocular portion of the primary visual cortex for further analysis, a region of interest (ROI) was automatically calculated on the mean image of the response by selecting the pixels in the lowest 30% ΔR/R of the range between the maximal and minimal intensity pixel 26. To weaken background fluctuations a manually selected polygonal region of reference (ROR) was subtracted. The ROR was placed where no clear response, blood vessel artifact or irregularities of the skull were observed 27. Mean evoked responses were quantitatively estimated as the average intensity inside the ROI.

Electrophysiology

Primary neuronal cell culture: experiments were performed on cortical neurons obtained from 18-day old embryos of both Cdkl5+/y and Cdkl5$^{-/y}$ mice. The S1 cortex was rapidly dissected under sterile conditions, kept in cold HBSS (4°C) with high glucose, and then digested with papain (0,5 mg/ml) dissolved in HBSS plus DNase (0,1 mg/ml). Isolated cells were then plated at the final density of 1200 cells/mm2. The cells were incubated with 1% penicillin/streptomycin, 1% glutamax, 2.5% fetal bovine serum, 2% B-27 supplemented neurobasal medium in a humidified 5% CO2 atmosphere at 37°C. Experiments were performed at DIV 16 - 18.

Patch clamp: experiments were performed in voltage clamp conditions and whole-cell configuration as in 28. Patch electrodes, fabricated from thick borosilicate glasses (Hilgenberg, Mansifield, Germany), were pulled to a final resistance of 3-5 M ngs. Patch Clamp reco performed in whole cell configuration using a Multiclamp 700-B amplifier connected to a Digidata 1440 and governed by the pClamp10 software (Axon Instruments, Molecular Devices Ltd, USA). NMDAR activated currents were recorded by holding neurons at -70 mV and perfusing them with the NMDAR agonist, N-Methyl-D-aspartate, (NMDA, 50 µM). The external solution contained (in mM): 130 NaCl, 1.8 CaCl2, 10 HEPES, 10 glucose, 1.2 Glycine (pH 7.4). The internal solution contained (in mM): 90 CsCl, 20 TEACl, 10 glucose, 1 MgCl, 4 ATP, 0,5 GTP, 15 phosphocreatine (pH 7.4). These experiments were performed in the presence of the AMPA and GABAa receptors blockers 6,7-dinitroquinoxaline-2,3-dione, DNQX (20 µM, Sigma-Aldrich) and picrotoxin (100 µM), respectively. Tetrodotoxin (TTX 0.3 µM) was added to block voltage-gated Na+ channels. The mGluR5 were selectively activated for 2 min either by the agonist DHPG (100 µM) or the positive allosteric modulator CDPPB (10 µM).

Miniature post-synaptic currents (mPSCs) will be recorded by by holding neurons at -70 mV, recording for 120 seconds, and superfusing the postsynaptic neuron with a Tyrode's solution containing (in mM): 2 CaCl2, 130 NaCl, 2 MgCl2, 10 HEPES, 4 KCl, and 10 glucose, pH 7.4. The standard internal solution was (in mM): 90 CsCl, 20 TEA-Cl, 10 EGTA, 10 glucose, 1 MgCl2, 4 ATP, 0.5 GTP, and 15 phosphocreatine, pH 7.4. Picrotoxin is added to the Tyrode solution to block GABA A-dependent currents. Tetrodotoxin (TTX) will be added for the measure of miniature postsynaptic currents in order to block spontaneous action potentials propagation. Analysis of peak amplitudes and inter-spike intervals (ISI) was performed with Clampfit software (Axon Instruments). Miniature excitatory postsynaptic currents (mEPSCs) are analyzed through the Peak-scaled variance analysis (PSVA) in order to determine the unitary current and the number of postsynaptic receptors, as described by Traynelis et al. (1998), using MiniAnalysis programs

(version 6.0.1, Synaptosoft, Leonia, NJ) 29. The unitary current will be calculated by fitting the relationship between peak-scaled variance σ2(t) and the mean amplitude I(t) with the following equation: σ2(t)=iI(t)-(I2(t)/Nch)+ σB2, where is the weighted mean unitary current and Nch is the number of channels activated at the peak of mEPSCs. Cells were then treated for 2 minutes with DHPG (100 µM).

Behavioural analyses

For the acute treatment regime, 1h after a single i.p. injection with either CDPPB or vehicle, animals were probed with adhesive tape removal test and Y-maze test. For the subchronically treated mice, 24h after the last injection hind-limb clasping behaviour was tested.

Adhesive tape removal test: sensorimotor abilities were evaluated using the adhesive tape removal test as previously described. Briefly, P56 mice were habituated to the testing room for 30 min before starting the experiment and then single animals were placed in the testing cage for the habituation period of 60 sec. The animal was then removed from the testing box and an adhesive tape strip (0.3 cm x 0.4 cm) was placed on the bottom of one forepaw while the other one was lightly touched by the operator with the same pressure. Animals were put back in the testing cage and the latency to touch the tape was recorded with a cut off time of 2 min.

Y-maze test: spontaneous alternation test was used to evaluate spatial working memory in mice.

We used an in-house made Y maze that is composed of three arms (34 cm × 5 cm × 10 cm) angled at 120° from one another and made by gray opaque plastic material. Each mouse was placed at the centre of the maze where it can freely explore the three arms for 8 min. Arm entries were defined by the presence of all four paws in an arm. The percentage of spontaneous alternations was calculated as follows: (total alternations / total arm entries − 2) × 100.

Hind-limb clasping: the presence of hind-limb clasping behaviour was tested by suspending the mice from their tail for 2 min and video recorded. Hind-limb clasping scores were assessed as in (Amendola et al., 2014).

Statistical analysis

All data are reported as mean ± SEM. For the animal experiments, n = number of mice. All statistical analyses were performed using Prism software (Graphpad, La Jolla, CA, USA). For the in-vitro colocalization and co-IP experiments, one-way analysis of variance (ANOVA) followed by Fisher's post hoc test was used. For the in-vivo analyses, Student's t-test or two-way ANOVA followed by Fisher's LSD post hoc test were performed, as indicated in the text. For electrophysiology analyses Student's t-test and chi-square were used, as indicated in the text. All the raw data are reported in table S1. Statistical analysis and the n for each experimental group are reported in figure legends.

Table1. Mean ± SEM values for each statistical analysis

Figure 1			**Cdkl5 $^{+/y}$**	**Cdkl5 $^{-/y}$**
C	O.D mGluR5/Homer1bc		0.254 ± 0.062	0.174 ± 0.026
B	mGluR5^{+} puncta /100μm^2	LII-III	68.28 ± 6.23	51.20 ± 1.68
		L V	59.63 ± 3.19	46.01 ± 2.75
Figure 2			**Cdkl5 $^{+/y}$**	**Cdkl5 $^{-/y}$**
C	Peak amplitude (pA)		21.71 ± 1.51	21.95 ± 1.56
D	Inter-event interval (IEI)		200.8 ± 33.62	333.6 ± 54.95
E	%IEI	Control	100 ± 16.75	100 ± 16.47
		DHPG	329.3 ± 54.43	162.2 ± 34.90
G	NMDA current		869.60 ± 84.22	433.98 ± 88.09
H	% Change	DHPG	38.35 ± 16.96	-14.47± 13.32
I	% of cells with potentiated I_{NMDA}		73% (11/15 cells)	29% (4/14 cells)
K	% Changes	CDPPB	42.92 ± 10.27	45.19 ± 14.75
L	% of cells with potentiated I_{NMDA}		78% (13/18 cells)	83% (10/12 cells)

Figure 3				Vehicle		CDPPB	
				Cdkl5 $^{+/y}$	Cdkl5 $^{-/y}$	Cdkl5 $^{+/y}$	Cdkl5 $^{-/y}$
B	Amplitude (DR/R)	Baseline		-7.14 ± 1.21	-3.54 ± 0.32		-3.8 ± 0.53
		Post-injection			-3.29 ± 0.67		-5.77 ± 0.86
C	Time to contact (Sec)			31.33 ± 6.03	59.38 ± 6.39	42.70 ± 6.61	39.88 ± 8.88
D	% Alternation			67.03 ± 3.36	46.26 ± 3.63	64.21 ± 3.41	60.97 ± 3.19
E	Nr entrance			19.43 ± 1.87	18.29 ± 4.20	16.28 ± 2.33	22.43 ± 1.41
Figure 4				**Vehicle**		**CDPPB**	
				Cdkl5 $^{+/y}$	**Cdkl5 $^{-/y}$**	**Cdkl5 $^{+/y}$**	**Cdkl5 $^{-/y}$**
B	Homer1bc+ puncta/100μm ^{2}	S1	LII-III	82.13 ± 4.94	61.22 ± 4.23	83.40 ± 6.81	77.93 ± 7.61
			L V	77.15 ± 2.82	59.40 ± 4.41	76.22 ± 7.42	72.08 ± 5.77
		V1	LII-III	92.80 ± 7.00	68.88 ± 1.81	103.1 ± 4.46	95.95 ± 6.21
			L V	96.00 ± 3.38	67.23 ± 3.03	90.38 ± 10.27	87.75 ± 6.81
C	mGluR5$^+$ puncta /100μm^2	S1	LII-III	83.72 ± 1.28	61.06 ± 2.86	88.37 ± 2.33	83.07 ± 5.56
			L V	80.00 ± 6.38	51.90 ± 1.91	81.63 ± 2.88	81.97 ± 1.97
		V1	LII-III	95.38 ± 4.74	65.87 ± 6.14	78.8 ± 9.70	93.72 ± 3.93
			L V	88.05 ± 4.64	57.14 ± 5.28	80.82 ± 9.99	78.63 ± 7.93
F	ARC$^+$ cells /mm^2		L I	0 ± 0	0 ± 0	0 ± 0	0 ± 0
			L II-III	103.5 ± 20.75	41.19 ± 14.8	131.5 ± 63.43	127.3 ± 5.38
			L IV	365.9 ± 74.42	81.62 ± 18.1	251.6 ± 179.3	296.5 ±133.9
			L V	255.8 ± 40.13	91.2 ± 19.97	389.4 ± 221.6	367.7 ± 20.3
			L VI	672.1 ± 83.87	470.9 ± 60.24	998.0 ± 90.15	1031 ± 140.5
			L I-VI	346.7 ± 45.87	184.1 ± 4.37	453.9 ± 117.8	467.60 ± 98.39
Figure 5				**Vehicle**		**CDPPB**	
				Cdkl5 $^{+/y}$	**Cdkl5 $^{-/y}$**	**Cdkl5 $^{+/y}$**	**Cdkl5 $^{-/y}$**
B	Homer1bc+ puncta/100μm^2		LII-III	85.87 ± 3.58	61.63 ± 3.91	76.23 ± 3.87	80.07 ± 4.64
			L V	72.37 ± 3.43	51.10 ± 4.78	71.49 ± 3.95	67.31 ± 5.18
C	Clasping time (SEC)			0.00 ± 0.00	10.61 ± 2.38	0.00 ± 0.00	5.36 ± 1.76
E	c-FOS intensity		L I-VI	1.48 ± 0.22	0.88 ± 0.06	1.09 ± 0.26	1.05 ± 0.6
Figure 6				**C1**	**P1**	**C2**	**P2**
B	Homer1bc+ puncta/100μm^2			92.17	70.25	91.86	68.70
C	PSD95+ puncta/100μm^2			85.53	66.08	88.62	62.53
E	VGluT1+ puncta/100μm^2			59.70	39.1	50.3	38.8
G	mGluR5/Act			0.85	0.65	0.33	0.08

Table2. Specificity of antibodies used in the manuscript

Primary Antibody	**Species of origin**	**Working dilution**			**Supplier and catalog no.**
		WB	**IF**	**IP**	

Homer1bc	Rabbit	1:1000	1:500		Synaptic System, Germany, cod. 160 023
Homer1bc	Mouse			1 mg	Santa Cruz Biotechnology, cod. sc-25271
mGluR5	Rabbit	1:500	1:250		Millipore, Germany, USA cod. AB5675
ARC	Rabbit		1:500		Synaptic System, Germany, cod. 156 003
c-FOS	Rabbit		1:1500		Santa Cruz Biotechnology, USA, cat. sc-52
PSD-95	Mouse	1:500	1:250		Neuromab; CA, USA, Clone K28/43
VGluT1	Guinea pig		1:5000		Millipore, Germany, cat. 5905

Supplementary Materials:

Fig. S1

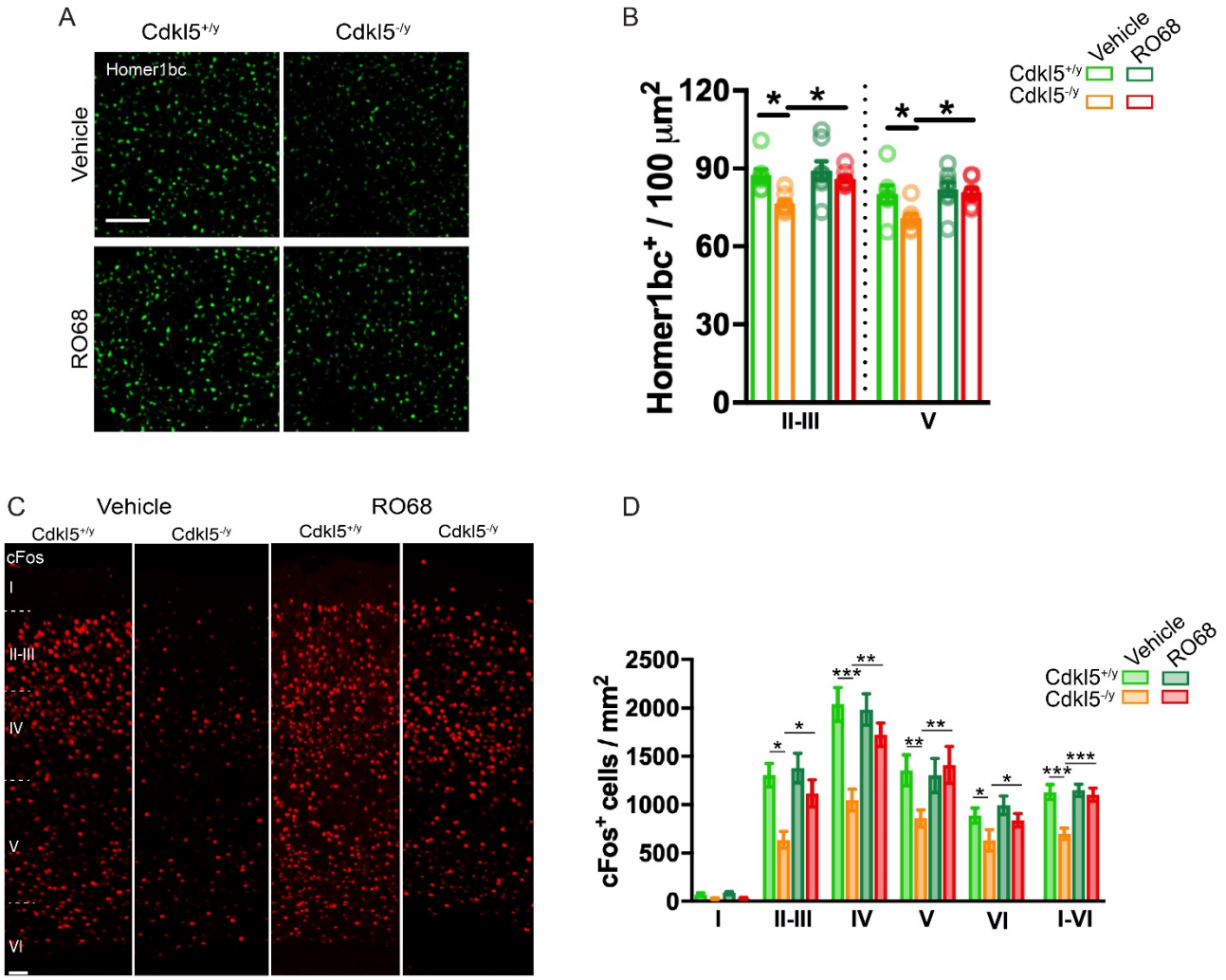

Figure S1. Acute administration of RO6807794 (RO68) rescues the morpho-functional defects shown by Cdkl5$^{-/y}$ mice. *(**A**) Representative confocal images showing Homer1bc^{+} puncta in layer II-III of S1 cortex from either vehicle- or RO68-treated Cdkl5$^{+/y}$ and Cdkl5$^{-/y}$ mice (scale bar: 5 µm). (**B**) Histograms showing differences between genotypes in Homer1bc^{+} immunopuncta density counted from layers II-III and V of S1 cortices in either vehicle- or RO68-treated mice. (**C**) Confocal images of c-FOS^{+} immunostaining in sections of the S1 cortex from Cdkl5$^{+/y}$ and Cdkl5$^{-/y}$ mice, treated with vehicle or RO68 (scale bar: 50 µm), and relative cFOS^{+} cells density*

*quantitation (**D**) throughout layers of V1 cortex. Two-way ANOVA followed by Fisher's multiple comparison test, *p < 0.05, ** p < 0.01, *** p < 0.001; (n = 8 animals for each genotype).*

MATERIALS AND METHODS FOR SUPPLEMENTARY DATA:

Drug administration: 0.3 mg/kg of RO6807794 was injected intraperitonially. The drug was prepared always fresh by dissolving it in 0.3% of Tween 80 and the volume was made up with normal saline. The experimental plan included four groups of mice, i.e.: WT mice treated with vehicle; WT mice treated with RO68; Cdkl5 KO mice treated with vehicle and Cdkl5 KO mice treated with RO68. Two hours after the treatment, the animals were sacrificed, and brains were taken for immunofluorescence (see below).

Immunofluorescence and Images acquisition and analysis: see the relevant methods section in the main text.

Acknowledgments: ???

Author's contribution: AG and MG conceived and designed the study. AG, RP performed the experiments. LL, GS, RM, EP performed IOS experiments. SG performed experiments on human tissues, AG, RP, NM, FP performed behavioural experiments, AG performed immunofluorescence experiments. AM and GC performed electrophysiological experiments. CS, AN synthesized and provided RO6807794; AG, RP, AR, TP, AM and MG analyzed the data. AG, RP, AR and MG wrote the manuscript.

Funding: This work was supported by research grants from: University of Pennsylvania Orphan Disease Center on behalf of LouLou Foundation (CDKL5 PILOT GRANT PROGRAM n. CDKL5 - 17 - 106 – 01) and from Associazione CDKL5 Insieme verso la cura (Italy) to MG and TP; The International Foundation for CDKL5 Research, Associazione Albero di Greta and Fondazione CRT (n. 2018.0889) and by Fondazione Telethon Grant (n. GGP15098) to M.G..

Institutional Review Board Statement: The study was conducted in accordance with European Community Council Directive 2010/63/UE for care and use of experimental animals with protocols approved by the Italian Minister for Scientific Research (Authorization number 38/2020-PR) and the Bioethics Committee of the University of Torino, Italy.

Conflicts of Interest: The authors do not have financial disclosures or conflict of interest to declare.

References

Alfieri A, Sorokina O, Adrait A, Angelini C, Russo I, Morellato A, Matteoli M, Menna E, Boeri Erba E, McLean C, Armstrong JD, Ala U, Buxbaum JD, Brusco A, Couté Y, De Rubeis S, Turco E, Defilippi P. Synaptic Interactome Mining Reveals p140Cap as a New Hub for PSD Proteins Involved in Psychiatric and Neurological Disorders. Front Mol Neurosci. 2017 Jun 30;10:212. doi: 10.3389/fnmol.2017.00212. PMID: 28713243; PMCID: PMC5492163.

Aloisi E, Le Corf K, Dupuis J, Zhang P, Ginger M, Labrousse V, Spatuzza M, Georg Haberl M, Costa L, Shigemoto R, Tappe-Theodor A, Drago F, Vincenzo Piazza P, Mulle C, Groc L, Ciranna L, Catania MV, Frick A. 2017. Altered surface mGluR5 dynamics provoke synaptic NMDAR dysfunction and cognitive defects in Fmr1 knockout mice. *Nat Commun* **8**:1103. doi:10.1038/s41467-017-01191-2

Amendola E, Zhan Y, Mattucci C, Castroflorio E, Calcagno E, Fuchs C, Lonetti G, Silingardi D, Vyssotski AL, Farley D, Ciani E, Pizzorusso T, Giustetto M, Gross CT. 2014. Mapping pathological phenotypes in a mouse model of CDKL5 disorder. *PLoS One* **9**:5–16. doi:10.1371/journal.pone.0091613

Ango F, Pin JP, Tu JC, Xiao B, Worley PF, Bockaert J, Fagni L. 2000. Dendritic and axonal targeting of type 5 metabotropic glutamate receptor is regulated by Homer1 proteins and neuronal excitation. *J Neurosci* **20**:8710–8716.

Auerbach BD, Osterweil EK, Bear MF. 2011. Mutations causing syndromic autism define an axis of synaptic pathophysiology. *Nature* **480**:63–68. doi:10.1038/nature10658

Ballester-Rosado CJ, Sun H, Huang JY, Lu HC. 2016. mGluR5 exerts cell-autonomous influences on the functional and anatomical development of layer IV cortical neurons in the mouse primary somatosensory cortex. *J Neurosci* **36**:8802–8814.

doi:10.1523/JNEUROSCI.1224-16.2016

Baltussen LL, Negraes PD, Silvestre M, Claxton S, Moeskops M, Christodoulou E, Flynn HR, Snijders AP, Muotri AR, Ultanir SK. 2018. Chemical genetic identification of CDKL5 substrates reveals its role in neuronal microtubule dynamics. *EMBO J* **37**:e99763. doi:10.15252/embj.201899763

Barbiero I, Peroni D, Tramarin M, Chandola C, Rusconi L, Landsberger N, Kilstrup-Nielsen C. 2017. The neurosteroid pregnenolone reverts microtubule derangement induced by the loss of a functional CDKL5-IQGAP1 complex. *Hum Mol Genet* **26**:3520–3530. doi:10.1093/hmg/ddx237

Bellone C, Lüscher C, Mameli M. 2008. Mechanisms of synaptic depression triggered by metabotropic glutamate receptors. *Cell Mol Life Sci* **65**:2913–2923. doi:10.1007/s00018-008-8263-3

Bouet V, Boulouard M, Toutain J, Divoux D, Bernaudin M, Schumann-Bard P, Freret T. 2009. The adhesive removal test: A sensitive method to assess sensorimotor deficits in mice. *Nat Protoc* **4**:1560–1564. doi:10.1038/nprot.2009.125

Chen C-C, Lu H-C, Brumberg JC. 2012. mGluR5 knockout mice display increased dendritic spine densities. *Neurosci Lett* **524**:65–68. doi:10.1016/J.NEULET.2012.07.014

Chen Y, Goudet C, Pin J-P, Conn PJ. 2008. N-{4-Chloro-2-[(1,3-dioxo-1,3-dihydro-2H-isoindol-2-yl)methyl]phenyl}-2-hydroxybenzamide (CPPHA) acts through a novel site as a positive allosteric modulator of group 1 metabotropic glutamate receptors. *Mol Pharmacol* **73**:909–18. doi:10.1124/mol.107.040097

Della Sala G, Putignano E, Chelini G, Melani R, Calcagno E, Michele Ratto G, Amendola E, Gross CT, Giustetto M, Pizzorusso T. 2016. Dendritic Spine Instability in a Mouse Model of

CDKL5 Disorder Is Rescued by Insulin-like Growth Factor 1. *Biol Psychiatry* **80**:302–311. doi:10.1016/j.biopsych.2015.08.028

Demarest S, Pestana-Knight EM, Olson HE, Downs J, Marsh ED, Kaufmann WE, Partridge C-A, Leonard H, Gwadry-Sridhar F, Frame KE, Cross JH, Chin RFM, Parikh S, Panzer A, Weisenberg J, Utley K, Jaksha A, Amin S, Khwaja O, Devinsky O, Neul JL, Percy AK, Benke TA. 2019. Severity Assessment in CDKL5 Deficiency Disorder. *Pediatr Neurol* **97**:38–42. doi:10.1016/J.PEDIATRNEUROL.2019.03.017

Demarest ST, Olson HE, Moss A, Pestana-Knight E, Zhang X, Parikh S, Swanson LC, Riley KD, Bazin GA, Angione K, Niestroj L, Lal D, Juarez-Colunga E, Benke TA. 2019. CDKL5 deficiency disorder: Relationship between genotype, epilepsy, cortical visual impairment, and development. *Epilepsia* **60**:1733–1742. doi:10.1111/epi.16285

Edfawy M, Guedes JR, Pereira MI, Laranjo M, Carvalho MJ, Gao X, Ferreira PA, Caldeira G, Franco LO, Wang D, Cardoso AL, Feng G, Carvalho AL, Peça J. 2019. Abnormal mGluR-mediated synaptic plasticity and autism-like behaviours in Gprasp2 mutant mice. *Nat Commun* **10**:1431. doi:10.1038/s41467-019-09382-9

Fuchs C, Trazzi S, Torricella R, Viggiano R, De Franceschi M, Amendola E, Gross C, Calz?? L, Bartesaghi R, Ciani E. 2014. Loss of CDKL5 impairs survival and dendritic growth of newborn neurons by altering AKT/GSK-3?? signaling. *Neurobiol Dis* **70**:53–68. doi:10.1016/j.nbd.2014.06.006

Giuffrida R, Musumeci S, D'Antoni S, Bonaccorso CM, Giuffrida-Stella AM, Oostra BA, Catania MV. 2005. A reduced number of metabotropic glutamate subtype 5 receptors are associated with constitutive Homer proteins in a mouse model of fragile X syndrome. *J Neurosci* **25**:8908–8916. doi:10.1523/JNEUROSCI.0932-05.2005

Gogliotti RG, Senter RK, Rook JM, Ghoshal A, Zamorano R, Malosh C, Stauffer SR, Bridges TM, Bartolome JM, Daniels JS, Jones CK, Lindsley CW, Conn PJ, Niswender CM. 2016. mGlu $_5$ positive allosteric modulation normalizes synaptic plasticity defects and motor phenotypes in a mouse model of Rett syndrome. *Hum Mol Genet* **25**:1990–2004. doi:10.1093/hmg/ddw074

Grasso S, Chapelle J, Salemme V, Aramu S, Russo I, Vitale N, Verdun di Cantogno L, Dallaglio K, Castellano I, Amici A, Centonze G, Sharma N, Lunardi S, Cabodi S, Cavallo F, Lamolinara A, Stramucci L, Moiso E, Provero P, Albini A, Sapino A, Staaf J, Di Fiore PP, Bertalot G, Pece S, Tosoni D, Confalonieri S, Iezzi M, Di Stefano P, Turco E, Defilippi P. The scaffold protein p140Cap limits ERBB2-mediated breast cancer progression interfering with Rac GTPase-controlled circuitries. Nat Commun. 2017 Mar 16;8:14797. doi: 10.1038/ncomms14797. Erratum in: Nat Commun. 2018 Mar 30;9:16203. PMID: 28300085; PMCID: PMC5357316.

Guo W, Wei F, Zou S, Robbins MT, Sugiyo S, Ikeda T, Tu J-C, Worley PF, Dubner R, Ren K. 2004. Group I metabotropic glutamate receptor NMDA receptor coupling and signaling cascade mediate spinal dorsal horn NMDA receptor 2B tyrosine phosphorylation associated with inflammatory hyperalgesia. *J Neurosci* **24**:9161–73. doi:10.1523/JNEUROSCI.3422-04.2004

Hering H, Sheng M. 2001. Dendritic spines: structure, dynamics and regulation. *Nat Rev Neurosci* **2**:880–888. doi:10.1038/35104061

Kameshita I, Sekiguchi M, Hamasaki D, Sugiyama Y, Hatano N, Suetake I, Tajima S, Sueyoshi N. 2008. Cyclin-dependent kinase-like 5 binds and phosphorylates DNA methyltransferase 1. *Biochem Biophys Res Commun* **377**:1162–1167. doi:10.1016/J.BBRC.2008.10.113

Kelly E, Schaeffer SM, Dhamne SC, Lipton JO, Lindemann L, Honer M, Jaeschke G, Super CE, Lammers SH, Modi ME, Silverman JL, Dreier JR, Kwiatkowski DJ, Rotenberg A, Sahin M. 2018. MGluR5 Modulation of Behavioral and Epileptic Phenotypes in a Mouse Model of Tuberous Sclerosis Complex. *Neuropsychopharmacology* **43**:1457–1465. doi:10.1038/npp.2017.295

Kinney GG, O'Brien JA, Lemaire W, Burno M, Bickel DJ, Clements MK, Chen T-B, Wisnoski DD, Lindsley CW, Tiller PR, Smith S, Jacobson MA, Sur C, Duggan ME, Pettibone DJ, Conn PJ, Williams DL. 2005. A novel selective positive allosteric modulator of metabotropic glutamate receptor subtype 5 has in vivo activity and antipsychotic-like effects in rat behavioral models. *J Pharmacol Exp Ther* **313**:199–206. doi:10.1124/jpet.104.079244

Komotar RJ, Kim GH, Sughrue ME, Otten ML, Rynkowski MA, Kellner CP, Hahn DK, Merkow MB, Garrett MC, Starke RM, Connolly ES. 2007. Neurologic assessment of somatosensory dysfunction following an experimental rodent model of cerebral ischemia. *Nat Protoc* **2**:2345–2347. doi:10.1038/nprot.2007.359

Lujan R, Nusser Z, Roberts JD, Shigemoto R, Somogyi P. 1996. Perisynaptic location of metabotropic glutamate receptors mGluR1 and mGluR5 on dendrites and dendritic spines in the rat hippocampus. *Eur J Neurosci* **8**:1488–1500. doi:10.1111/j.1460-9568.1996.tb01611.x

Lupori L, Sagona G, Fuchs C, Mazziotti R, Stefanov A, Putignano E, Napoli D, Strettoi E, Ciani E, Pizzorusso T. 2019. Site-specific abnormalities in the visual system of a mouse model of CDKL5 deficiency disorder. *Hum Mol Genet* **28**:2851–2861. doi:10.1093/hmg/ddz102

Mari F, Azimonti S, Bertani I, Bolognese F, Colombo E, Caselli R, Scala E, Longo I, Grosso S, Pescucci C, Ariani F, Hayek G, Balestri P, Bergo A, Badaracco G, Zappella M, Broccoli V, Renieri A, Kilstrup-Nielsen C, Landsberger N. 2005. CDKL5 belongs to the same molecular

pathway of MeCP2 and it is responsible for the early-onset seizure variant of Rett syndrome. *Hum Mol Genet* **14**:1935–1946. doi:10.1093/hmg/ddi198

Mazziotti R, Lupori L, Sagona G, Gennaro M, Sala G Della, Putignano E, Pizzorusso T. 2017. Searching for biomarkers of CDKL5 disorder: early-onset visual impairment in CDKL5 mutant mice. *Hum Mol Genet* **26**:2290–2298. doi:10.1093/hmg/ddx119

Mellone M, Stanic J, Hernandez LF, Iglesias E, Zianni E, Longhi A, Prigent A, Picconi B, Calabresi P, Hirsch EC, Obeso JA, Di Luca M, Gardoni F. NMDA receptor GluN2A/GluN2B subunit ratio as synaptic trait of levodopa-induced dyskinesias: from experimental models to patients. Front Cell Neurosci. 2015 Jul 6;9:245. doi: 10.3389/fncel.2015.00245. PMID: 26217176; PMCID: PMC4491616.

Ménard C, Quirion R. 2012. Successful cognitive aging in rats: A role for mGluR5 glutamate receptors, homer 1 proteins and downstream signaling pathways. *PLoS One* **7**:e28666. doi:10.1371/journal.pone.0028666

Moult PR, Gladding CM, Sanderson TM, Fitzjohn SM, Bashir ZI, Molnar E, Collingridge GL. 2006. Tyrosine phosphatases regulate AMPA receptor trafficking during metabotropic glutamate receptor-mediated long-term depression. *J Neurosci* **26**:2544–2554. doi:10.1523/JNEUROSCI.4322-05.2006

Muñoz IM, Morgan ME, Peltier J, Weiland F, Gregorczyk M, Cm Brown F, Macartney T, Toth R, Trost M, Rouse J. 2018. Phosphoproteomic screening identifies physiological substrates of the CDKL5 kinase. *EMBO J* **37**:e99559.

Nawaz MS, Giarda E, Bedogni F, La Montanara P, Ricciardi S, Ciceri D, Alberio T, Landsberger N, Rusconi L, Kilstrup-Nielsen C. 2016. CDKL5 and Shootin1 Interact and Concur in Regulating Neuronal Polarization. *PLoS One* **11**:e0148634.

doi:10.1371/journal.pone.0148634

Negraes PD, Trujillo CA, Yu N-K, Wu W, Yao H, Liang N, Lautz JD, Kwok E, McClatchy D, Diedrich J, de Bartolome SM, Truong J, Szeto R, Tran T, Herai RH, Smith SEP, Haddad GG, Yates JR, Muotri AR. 2021. Altered network and rescue of human neurons derived from individuals with early-onset genetic epilepsy. *Mol Psychiatry*. doi:10.1038/s41380-021-01104-2

Oh WC, Hill TC, Zito K. 2013. Synapse-specific and size-dependent mechanisms of spine structural plasticity accompanying synaptic weakening. *Proc Natl Acad Sci U S A* **110**:E305-12. doi:10.1073/pnas.1214705110

Okuda K, Kobayashi S, Fukaya M, Watanabe A, Murakami T, Hagiwara M, Sato T, Ueno H, Ogonuki N, Komano-Inoue S, Manabe H, Yamaguchi M, Ogura A, Asahara H, Sakagami H, Mizuguchi M, Manabe T, Tanaka T. 2017. CDKL5 controls postsynaptic localization of GluN2B-containing NMDA receptors in the hippocampus and regulates seizure susceptibility. *Neurobiol Dis* **106**:157–170. doi:10.1016/j.nbd.2017.07.002

Perroy J, Raynaud F, Homburger V, Rousset M-C, Telley L, Bockaert JL, Fagni L. 2008. Direct Interaction Enables Cross-talk between Ionotropic and Group I Metabotropic Glutamate Receptors. *J Biol Chem* **283**:6799–805. doi:10.1074/jbc.M705661200

Piers TM, Kim DH, Kim BC, Regan P, Whitcomb DJ, Cho K. 2012. Translational concepts of mglur5 in synaptic diseases of the brain. *Front Pharmacol* **3 NOV**:1–7. doi:10.3389/fphar.2012.00199

Pizzo R, Gurgone A, Castroflorio E, Amendola E, Gross C, Sassoè-Pognetto M, Giustetto M. 2016. Lack of Cdkl5 Disrupts the Organization of Excitatory and Inhibitory Synapses and Parvalbumin Interneurons in the Primary Visual Cortex. *Front Cell Neurosci* **10**:261.

doi:10.3389/fncel.2016.00261

Pizzo R, Lamarca A, Sassoè-Pognetto M, Giustetto M. 2019. Structural Bases of Atypical Whisker Responses in a Mouse Model of CDKL5 Deficiency Disorder. *Neuroscience* **95**. doi:10.1016/j.neuroscience.2019.08.033

Reiner A, Levitz J. 2018. Glutamatergic Signaling in the Central Nervous System: Ionotropic and Metabotropic Receptors in Concert. *Neuron* **98**:1080–1098. doi:10.1016/J.NEURON.2018.05.018

Ricciardi S, Ungaro F, Hambrock M, Rademacher N, Stefanelli G, Brambilla D, Sessa A, Magagnotti C, Bachi A, Giarda E, Verpelli C, Kilstrup-Nielsen C, Sala C, Kalscheuer VM, Broccoli V. 2012. CDKL5 ensures excitatory synapse stability by reinforcing NGL-1-PSD95 interaction in the postsynaptic compartment and is impaired in patient iPSC-derived neurons. *Nat Cell Biol* **14**:911–23. doi:10.1038/ncb2566

Ronesi JA, Collins KA, Hays SA, Tsai N-P, Guo W, Birnbaum SG, Hu J-H, Worley PF, Gibson JR, Huber KM. 2012. Disrupted Homer scaffolds mediate abnormal mGluR5 function in a mouse model of fragile X syndrome. *Nat Neurosci* **15**:431–40, S1. doi:10.1038/nn.3033

Rusconi L, Salvatoni L, Giudici L, Bertani I, Kilstrup-Nielsen C, Broccoli V, Landsberger N. 2008. CDKL5 expression is modulated during neuronal development and its subcellular distribution is tightly regulated by the C-terminal tail. *J Biol Chem* **283**:30101–11. doi:10.1074/jbc.M804613200

Sala C, Futai K, Yamamoto K, Worley PF, Hayashi Y, Sheng M. 2003. Inhibition of Dendritic Spine Morphogenesis and Synaptic Transmission by Activity-Inducible Protein Homer1a. *J Neurosci* **23**:6327–6337. doi:23/15/6327 [pii]

Scheefhals N, MacGillavry HD. 2018. Functional organization of postsynaptic glutamate

receptors. *Mol Cell Neurosci* **91**:82–94. doi:10.1016/J.MCN.2018.05.002

Tomassy GS, Morello N, Calcagno E, Giustetto M. Developmental abnormalities of cortical interneurons precede symptoms onset in a mouse model of Rett syndrome. J Neurochem. 2014 Oct;131(1):115-27. doi: 10.1111/jnc.12803. Epub 2014 Aug 5. PMID: 24978323.

Tramarin M, Rusconi L, Pizzamiglio L, Barbiero I, Peroni D, Scaramuzza L, Guilliams T, Cavalla D, Antonucci F, Kilstrup-Nielsen C. 2018. The antidepressant tianeptine reverts synaptic AMPA receptor defects caused by deficiency of CDKL5. *Hum Mol Genet* **27**:2052–2063. doi:10.1093/hmg/ddy108

Trazzi S, Fuchs C, Viggiano R, De Franceschi M, Valli E, Jedynak P, Hansen FK, Perini G, Rimondini R, Kurz T, Bartesaghi R, Ciani E. 2016. HDAC4: a key factor underlying brain developmental alterations in CDKL5 disorder. *Hum Mol Genet* **25**:3887–3907. doi:10.1093/hmg/ddw231

Tu JC, Xiao B, Naisbitt S, Yuan JP, Petralia RS, Brakeman P, Doan A, Aakalu VK, Lanahan AA, Sheng M, Worley PF. 1999. Coupling of mGluR/Homer and PSD-95 Complexes by the Shank Family of Postsynaptic Density Proteins. *Neuron* **23**:583–592.

Verpelli C, Dvoretskova E, Vicidomini C, Rossi F, Chiappalone M, Schoen M, Di Stefano B, Mantegazza R, Broccoli V, Böckers TM, Dityatev A, Sala C. 2011. Importance of Shank3 protein in regulating metabotropic glutamate receptor 5 (mGluR5) expression and signaling at synapses. *J Biol Chem* **286**:34839–50. doi:10.1074/jbc.M111.258384

Vicidomini C, Ponzoni L, Lim D, Schmeisser M, Reim D, Morello N, Orelanna D, Tozzi A, Durante V, Scalmani P, Mantegazza M, Genazzani AA, Giustetto M, Sala M, Calabresi P, Boeckers TM, Sala C, Verpelli C. 2017. Pharmacological enhancement of mGlu5 receptors rescues behavioral deficits in SHANK3 knock-out mice Europe PMC Funders Group. *Mol*

Psychiatry **22**:689–702.

Wang H, Zhuo M. 2012. Group I metabotropic glutamate receptor-mediated gene transcription and implications for synaptic plasticity and diseases. *Front Pharmacol* **3**:189. doi:10.3389/fphar.2012.00189

Wang I-TJ, Allen M, Goffin D, Zhu X, Fairless AH, Brodkin ES, Siegel SJ, Marsh ED, Blendy JA, Zhou Z. 2012. Loss of CDKL5 disrupts kinome profile and event-related potentials leading to autistic-like phenotypes in mice. *Proc Natl Acad Sci U S A* **109**:21516–21. doi:10.1073/pnas.1216988110

Yennawar M, White RS, Jensen FE. 2019. Neurobiology of Disease AMPA Receptor Dysregulation and Therapeutic Interventions in a Mouse Model of CDKL5 Deficiency Disorder. doi:10.1523/JNEUROSCI.2041-18.2019

Zhu Y-C, Li D, Wang L, Lu B, Zheng J, Zhao S-L, Zeng R, Xiong Z-Q. 2013. Palmitoylation-dependent CDKL5-PSD-95 interaction regulates synaptic targeting of CDKL5 and dendritic spine development. *Proc Natl Acad Sci U S A* **110**:9118–23. doi:10.1073/pnas.1300003110